

**NASA  
Technical  
Memorandum**

NASA TM - 100352

IMPROVED CAPABILITIES OF THE MULTISPECTRAL  
ATMOSPHERIC MAPPING SENSOR (MAMS)

By Gary J. Jedlovec, K. Bryan Batson,  
Robert J. Atkinson, Chris C. Moeller,  
W. Paul Menzel, and Mark W. James

Space Science Laboratory  
Science and Engineering Directorate

(NASA-TM-100352) IMPROVED CAPABILITIES OF  
THE MULTISPECTRAL ATMOSPHERIC MAPPING SENSOR  
(MAMS) (NASA) 80 p CSCI 14B

N89-20430

Unclas  
G3/35 0192501

January 1989



National Aeronautics and  
Space Administration

George C. Marshall Space Flight Center

|   |  |  |  |   |                       |
|---|--|--|--|---|-----------------------|
| 1. REPORT NO.<br>NASA TM-100352   |  | 2. GOVERNMENT ACCESSION NO.                              |  | 3. RECIPIENT'S CATALOG NO.                                      |                       |
| 4. TITLE AND SUBTITLE<br><br>Improved Capabilities of the Multispectral Atmospheric Mapping Sensor (MAMS)   |  |  |  | 5. REPORT DATE<br>January 1989                                  |                       |
|   |  |  |  | 6. PERFORMING ORGANIZATION CODE<br>ES43                         |                       |
| 7. AUTHOR(S) Gary J. Jedlovec, K. Bryan Batson, <sup>1</sup> Robert J. Atkinson, <sup>2</sup> Chris C. Moeller, <sup>3</sup> W. Paul Menzel, <sup>4</sup> and   |  |  |  | 8. PERFORMING ORGANIZATION REPORT #                             |                       |
| 9. PERFORMING ORGANIZATION NAME AND ADDRESS<br><br>George C. Marshall Space Flight Center<br>Marshall Space Flight Center, AL 35812   |  |  |  | 10. WORK UNIT NO.   |                       |
|   |  |  |  | 11. CONTRACT OR GRANT NO.                                       |                       |
| 12. SPONSORING AGENCY NAME AND ADDRESS<br><br>National Aeronautics & Space Administration<br>Washington, DC 20546   |  |  |  | 13. TYPE OF REPORT & PERIOD COVERED<br><br>Technical Memorandum |                       |
|   |  |  |  | 14. SPONSORING AGENCY CODE                                      |                       |
| 15. SUPPLEMENTARY NOTES Prepared by Earth Science & Applications Division, Space Science Laboratory, Science & Engineering Directorate.<br><sup>1</sup> Universities Space Research Association, <sup>2</sup> General Electric Company,<br><sup>3</sup> Space Science & Engineering Center, Univ. of Wisconsin-Madison, <sup>4</sup> NOAA   |  |  |  |   |                       |
| 16. ABSTRACT<br><br>NASA maintains a number of aircraft instruments in support of future flight programs. Scientific findings from data collected with these instruments have been particularly important over the last few years as the scientific justification of new instrumentation for NASA's Earth Observing System (Eos) was being formulated. The Multispectral Atmospheric Mapping Sensor (MAMS) is one such instrument which has made an impact on Eos instrumentation. This document serves as a follow-on report to NASA TM-86565 entitled "The Multispectral Atmospheric Mapping Sensor (MAMS): Instrument Description, Calibration, and Data Quality" and discusses changes to the instrument which have led to new capabilities and improved data quality through better signal-to-noise and more accurate calibration methods. This report summarizes the capabilities which will exist with MAMS through the next 3 to 5 years. |  |  |  |   |                       |
| 17. KEY WORDS<br>Spectral Response, Multispectral Imagery, Radiometric Calibration, Radiances, Planck Function, Single Sample Noise   |  |  |  | 18. DISTRIBUTION STATEMENT<br><br>Unclassified--Unlimited       |                       |
| 19. SECURITY CLASSIF. (of this report)<br><br>Unclassified  |  | 20. SECURITY CLASSIF. (of this page)<br><br>Unclassified |  | 21. NO. OF PAGES<br><br>80                                      | 22. PRICE<br><br>NTIS |

TABLE OF CONTENTS

|  | Page |
|--|------|
| Table of Contents.....   | iii  |
| List of Illustrations.....   | v    |
| List of Tables.....  | vii  |
| I. INTRODUCTION.....   | 1    |
| II. INSTRUMENT CHARACTERISTICS.....  | 2    |
| A. MAMS Configuration and Scan Geometry.....                                     | 2    |
| B. Instrument Changes.....   | 5    |
| III. CALIBRATION.....  | 16   |
| A. Visible Channel Calibration.....  | 16   |
| B. Infrared Channel Calibration.....   | 17   |
| C. Noise Estimates.....  | 24   |
| D. Relative and Absolute Accuracy.....   | 32   |
| IV. NAVIGATION OF DATA.....  | 42   |
| A. Data Sources.....   | 42   |
| B. Navigation Relationships.....   | 42   |
| C. Error Sources and Bias Correction.....  | 45   |
| V. FLIGHT INFORMATION.....   | 48   |
| A. Recent Flights.....   | 48   |
| B. Data Availability.....  | 48   |
| VI. SCIENCE APPLICATIONS.....  | 49   |
| A. Low-level Precipitable Water Determination.....                               | 49   |
| B. Relationship Between Surface Features, Clouds,<br>and Precipitable Water..... | 49   |

TABLE OF CONTENTS (continued)

|   | Page |
|---|------|
| C. MAMS/VAS Combined Precipitable Water and<br>Stability.....                             | 50   |
| D. MAMS/HIS Combined Products for Diagnostic<br>Investigations.....                       | 50   |
| E. Surface Skin Temperature and Emissivity Mapping.                                       | 51   |
| F. Four-dimensional Water Vapor Structures.....   | 51   |
| G. Sea-surface Temperature Estimation and Sediment<br>Mapping for Geomorphic Changes..... | 52   |
| Appendix A: List of Acronyms.....   | 53   |
| Appendix B: Visible Channel Calibration Values.....                                       | 54   |
| Appendix C: MAMS Flight Information.....  | 56   |
| Appendix D: Selected MAMS Flight Tracks.....  | 58   |
| Appendix E: MAMS Data Requests.....   | 66   |
| References.....   | 68   |
| Bibliography.....   | 70   |

## LIST OF ILLUSTRATIONS

| Figure | Title  | Page |
|--------|--|------|
| 1      | MAMS scan geometry.....  | 4    |
| 2      | Channel calibration data representative of the<br>1985 instrument configuration.....           | 7    |
| 3      | Channel calibration data representative of the<br>COHMEX instrument configuration of 1986..... | 8    |
| 4      | Channel calibration data representative of the<br>current instrument configuration.....        | 10   |
| 5      | Spectral response curves for the infrared<br>channels.....                                     | 12   |
| 6      | MAMS 3.7 micrometer imagery for 27 January 1988..  | 13   |
| 7      | MAMS 11.1 micrometer imagery for 27 January 1988.  | 14   |
| 8      | MAMS 12.5 micrometer imagery for 27 January 1988.  | 15   |
| 9      | Typical calibration curves for the MAMS infrared<br>channels.....                              | 21   |
| 10     | Plot of MAMS and HIS 6.5 micrometer data for<br>comparison.....                                | 33   |
| 11     | Plot of MAMS and HIS 11.1 micrometer data for<br>comparison.....                               | 34   |
| 12     | Plot of MAMS and HIS 12.5 micrometer data for<br>comparison.....                               | 35   |
| 13     | MAMS 11.1 micrometer imagery for 27 January 1988.  | 38   |
| 14     | AVHRR 10.8 micrometer imagery for<br>27 January 1988.....                                      | 39   |

LIST OF ILLUSTRATIONS (continued)

| Figure | Title   | Page |
|--------|---|------|
| 15     | Schematic diagram for navigation of MAMS imagery.                           | 44   |
| 16     | Schematic diagram for inverse navigation<br>procedure.....                  | 46   |
| D1     | MAMS flight tracks for June 15, 18, 19, and<br>26, 1986.....                | 59   |
| D2     | MAMS flight tracks for July 5, 1986.....                                    | 60   |
| D3     | MAMS flight tracks for July 8, 11, 12,<br>and 20, of 1986.....              | 61   |
| D4     | MAMS flight track for July 21, 1986.....                                    | 62   |
| D5     | MAMS flight tracks for June 2, 4, 5, and 6, of<br>1987.....                 | 63   |
| D6     | MAMS flight tracks for June 7, 1987 and<br>June 5, 10 and July 8, 1988..... | 64   |
| D7     | MAMS flight track for August 18, 25,<br>and 26, 1988.....                   | 65   |

## LIST OF TABLES

| Table | Title  | Page |
|-------|--|------|
| 1     | MAMS instrument configuration.....   | 3    |
| 2     | Visible channel characteristics.....   | 5    |
| 3     | Infrared channel characteristics.....  | 11   |
| 4     | Infrared half power wavenumbers and monochromaticity corrections.....              | 18   |
| 5     | Channel calibration values.....  | 20   |
| 6     | Infrared sensitivity. ....   | 22   |
| 7     | Error due to truncation of calibration values....                                  | 23   |
| 8     | Error due to digitization of scene data.....                                       | 24   |
| 9     | Total maximum error due to truncation.....   | 25   |
| 10    | Single sample noise for selected flights based on structure function analysis..... | 26   |
| 11    | Single sample noise for selected flights based on variance calculations.....       | 29   |
| 12    | Statistics for the MAMS versus HIS data comparisons.....                           | 36   |
| 13    | Statistics for the MAMS versus AVHRR data comparisons.....                         | 37   |
| 14    | Statistics for the MAMS versus VAS data comparisons.....                           | 41   |
| 15    | Root mean square navigation errors.....  | 47   |
| B1    | Visible channel calibration values for 1985 flights.....                           | 54   |

LIST OF TABLES (continued)

| Table | Title   | Page |
|-------|---|------|
| B2    | Visible channel calibration values<br>for 1986 flights..... | 54   |
| B3    | Visible channel calibration values<br>for 1987 flights..... | 55   |
| B4    | Visible channel calibration values<br>for 1988 flights..... | 55   |
| C1    | MAMS flight information for 1986.....                       | 56   |
| C2    | MAMS flight information for 1987.....                       | 57   |
| C3    | MAMS flight information for 1988.....                       | 57   |
| E1    | MAMS navigated data tape inventory.....                     | 66   |

## TECHNICAL MEMORANDUM

### IMPROVED CAPABILITIES OF THE MULTISPECTRAL ATMOSPHERIC MAPPING SENSOR (MAMS)

#### I. INTRODUCTION

NASA's high altitude research program maintains a number of research instruments in support of future flight programs (see NASA, 1988 for aircraft specifications and list of supported instruments). Scientific findings from this program have been particularly important over the last few years as the scientific justification of new instrumentation for NASA's Earth Observing System (Eos) was being formulated. As NASA proceeds with Eos, it is important that support of the high altitude research program be continued so that aircraft observations can be made which serve as calibration and reference data for these new measurements.

The Multispectral Atmospheric Mapping Sensor (MAMS) is one such instrument which has made an impact on Eos instrumentation. Unique measurements made in water vapor absorption bands and window regions of the earth's emission spectrum have led to plans for water vapor channels on the MODerate-resolution Imaging Spectrometer -Nadir (MODIS-N) (NASA, 1988a). This document serves as a follow on report to NASA TM-86565 entitled "The Multispectral Atmospheric Mapping Sensor (MAMS): Instrument Description, Calibration, and Data Quality" (referred to herein as Jedlovec et al., 1986a or as "the previous report") and discusses changes to the instrument which have led to new capabilities and improved data quality (Section II) and more accurate calibration methods (Section III). In order to provide a summary of the data collected with MAMS, a complete list of flight dates and locations (with flight track maps) is provided (Section V and Appendix C and D). Procedures for requesting this data are also provided in Appendix E.

For many applications, registration of MAMS imagery with landmarks is required. Section IV discusses how this imagery is navigated on the Man-computer Interactive Data Access System (McIDAS) (Suomi et al., 1983). Finally, in Section VI, research applications of the data are discussed and specific examples are presented to show the applicability of these measurements to NASA's Earth System Science (ESS) objectives (Wilson et al., 1988).

## II. INSTRUMENT CHARACTERISTICS

Several changes which directly affect data quality have been made to the MAMS since the previous report. (1) The axe blade scan mirror common to all Daedalus scanners was upgraded to a full aperture mirror. This change (September 1986) increased the amount of energy falling on the detectors thus increasing the signal to noise ratios in all channels (roughly by a factor of two). (2) Infrared channel data was quantized with 10 bits of precision (June 1987) as opposed to the previous 8 bits. (3) The electronics were changed in order to average channel counts for calibration over several points on the blackbodies. This change, along with (1), provided a more reliable channel signal from the blackbodies and reduced the sensitivity to detector and amplifier noise. (4) A channel in the shortwave infrared region of the spectrum centered at 3.7 micrometers can be substituted for the channel at 6.5 micrometers to increase the observing capabilities for surface temperature and thermal emissivity at fine spatial scales. (This change was initiated by Goddard Space Flight Center scientist Jim Spinhirne in order to sense radiation from cirrus clouds). Details of these changes are discussed below.

### A. MAMS Configuration and Scan Geometry

The instrument configurations for MAMS are presented in Table 1. The standard MAMS setup uses the 5.0 milliradian aperture and 6.25 rps scan mirror speed, although other options exist. This configuration provides optimal sensing for very high quality thermal measurements. Figure 1 shows the usual scan geometry for the instrument aboard a NASA high altitude aircraft. At a 20 kilometer nominal altitude, the nadir ground spot size is about 100 meters. The dimensions of the ground resolution cell (GR) for any point on the scan are given by Jedlovec et al. (1986a) as

$$GR_c = \alpha * H * \sec^2(\theta) \quad (1)$$

$$GR_a = \alpha * H * \sec(\theta) \quad (2)$$

for the across track and along track directions, respectively. In these equations H is the aircraft/scanner height above ground,  $\theta$  is the angle from nadir, and  $\alpha$  is the aperture size. Since the data stream during a scan is digitized at a fixed angular rate, use of the larger aperture results in about a 58% overlap from one instantaneous field of view (ifov) to the next across the scan. The aircraft movement (P) from one scan to the next is a function of aircraft velocity (V) and instrument scan speed (SS) as given by

$$P = V / SS \quad (3)$$

-----  
Table 1

MAMS Instrument Configurations

|                      |   |
|----------------------|---|
| Spectral Bands:      | 8 visible/near infrared <sup>a</sup><br>3 thermal infrared <sup>b</sup> |
| Roll Correction:     | +/-15.0 degrees   |
| Pixels per scanline: | 716   |
| Calibration sources: | 2 controlled blackbodies  |

1985

|                                     |                 |
|-------------------------------------|-----------------|
| Scan speed:                         | 12.5 rps        |
| Instantaneous field of view (ifov): | 2.5 milliradian |
| Ground resolution @20 km:           | 50.0 m at nadir |
| Total field of view (fov):          | 85.92 degrees   |
| Swath width @ 20 km(agl):           | 37.2 km         |
| Digitization:                       | 8 bit           |

February through August 1986<sup>c</sup>

|                                     |                  |
|-------------------------------------|------------------|
| Scan speed:                         | 6.25 rps         |
| Instantaneous field of view (ifov): | 5.0 milliradian  |
| Ground resolution @20 km:           | 100.0 m at nadir |
| Total field of view (fov):          | 85.92 degrees    |
| Swath width @ 20 km(agl):           | 37.2 km          |
| Digitization:                       | 8 bit            |

June 1987 through August 1988<sup>c</sup>

|                                     |                        |
|-------------------------------------|------------------------|
| Scan speed:                         | 6.25 rps               |
| Instantaneous field of view (ifov): | 5.0 milliradian        |
| Ground resolution @20 km:           | 100.0 m at nadir       |
| Total field of view (fov):          | 85.92 degrees          |
| Swath width @ 20 km(agl):           | 37.2 km                |
| Digitization:                       | 8 bit(vis), 10 bit(IR) |

- <sup>a</sup> One visible channel is lost when 10 bit thermal data is collected.  
<sup>b</sup> A redundant fourth channel may be selected with a different gain setting.  
<sup>c</sup> Either the 3.7 or 6.5 micrometer channel was available with the 11.1 and 12.5 micrometer bands.
-

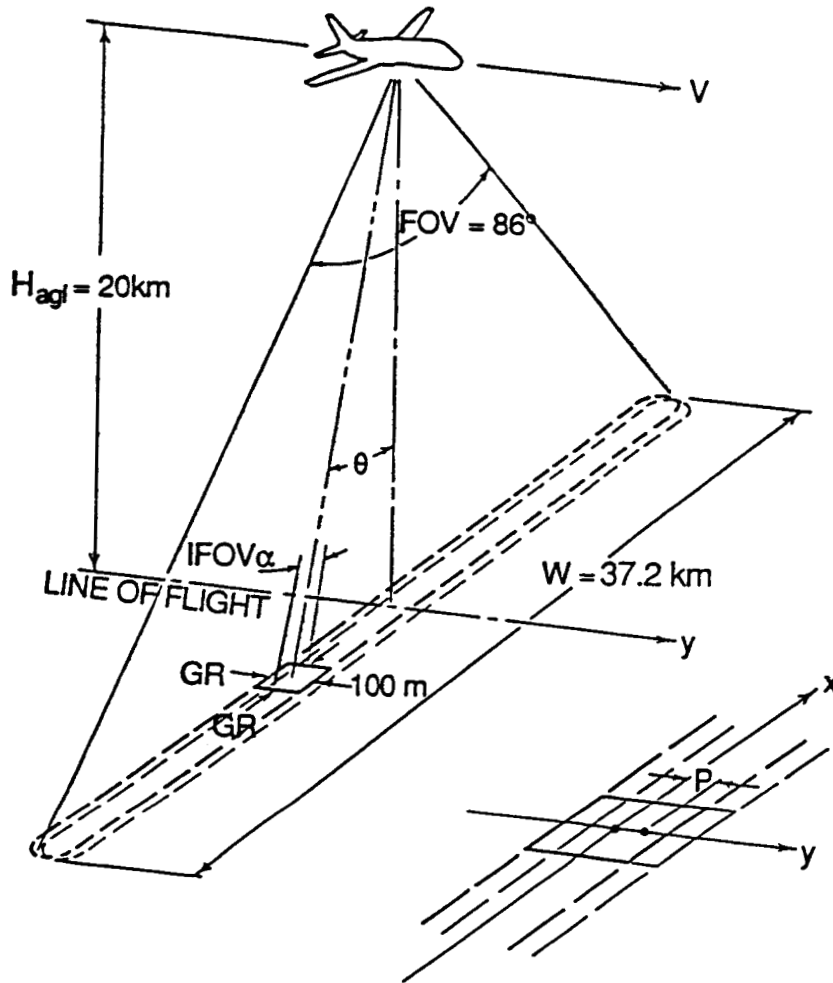


Figure 1. MAMS scan geometry from a high altitude aircraft platform. All numbers are nominal. Lower right insert shows the overlap of the ifovs from one scan line to the next. See text for further discussion.

For the standard MAMS configuration (5.0 mrad aperture, 6.25 rps, 20 km nominal height, and 206m/s air speed), the along track overlap is 66% of the field of view (66 m). When the overlapping pixels are all displayed, a somewhat "blurred" scene is available with 58 x 34 m resolution (at nadir). By sub-sampling the data during post-processing, 100 x 100m non-overlapping contiguous scan lines are available.

The use of the larger aperture changes the position of incident energy on the dispersing prism (see Jedlovec et al., 1986a for optical path diagram). This has the effect of changing the bandwidths for the visible and near infrared channels as shown in Table 2. Thus the use of the 5.0 milliradian aperture reduces the similarity of the visible channels with those of Landsat. The impact of this on applications of the visible data has not been evaluated.

-----

Table 2

Visible channel spectral characteristics for the 2.5 and 5.0 milliradian apertures (from Jedlovec et al., 1986a).

| Channel        | Bandwidth (@ 50% response) |                          |
|----------------|----------------------------|--------------------------|
|                | 2.5 mrad                   | 5.0 mrad                 |
| 1 <sup>a</sup> | 0.42 - 0.45                | 0.42 - 0.45              |
| 2              | 0.45 - 0.52 <sup>b</sup>   | 0.45 - 0.52 <sup>b</sup> |
| 3              | 0.52 - 0.60 <sup>b</sup>   | 0.52 - 0.60 <sup>b</sup> |
| 4              | 0.60 - 0.62                | 0.57 - 0.67              |
| 5              | 0.63 - 0.69 <sup>b</sup>   | 0.60 - 0.73 <sup>b</sup> |
| 6              | 0.69 - 0.75                | 0.65 - 0.83              |
| 7              | 0.76 - 0.90 <sup>b</sup>   | 0.72 - 0.99 <sup>b</sup> |
| 8              | 0.91 - 1.05                | 0.83 - 1.05              |

<sup>a</sup> Channel not available when 10 bit infrared data are collected.

<sup>b</sup> Similar to Landsat channel.

-----

### B. Instrument Changes

Variations in the counts from the blackbodies were the key calibration issue in the previous report. These variations were thought to be due to several factors. First, the small optics aperture, the axe blade mirror, and the rapid mirror scan speed were limiting factors in signal-to-noise. Second, a single sample from each blackbody was unrepresentative of the blackbody temperature. Third, irregular signals from the pre-amplifiers were causing sinusoidal fluctuations in the blackbody count values. Finally, truncation error associated with 8 bit data was significant.

In an attempt to reduce the variations in the calibration counts from the blackbodies, several changes were made to the instrument. The new scan mirror helped to stabilize the calibration values. In addition, the time constant (during which the blackbody signals are sensed in each channel) was increased to provide average count values which represented six adjacent spots (ifovs) on the face of the blackbodies. The replacement of the primary scan mirror required major modifications to the scan head. Since the scan head is used for the MAMS as well as the TMS and AOCI spectrometers, this change improved data quality in

all scanner applications. The mirror focused energy more effectively through the optical system and onto the detectors increasing the signal-to-noise values. An improvement in the quality of both the scene and calibration values was evident. Also, this change virtually eliminated the need for alignment of the primary optics (leaving just the alignment of the dewars into the optical path). Previous alignment problems had been apparent in early MAMS flights as a droop of the signal across the scan. This was also evident in 1986 COHMEX data (Jedlovec, 1987), and limited the quantitative calculations which could be performed with the data.

In June 1987, an interconnect printed circuit card was installed in the digitizer for use with MAMS. This card allowed utilization of 10 bit ADC (analog to digital converter) boards that were installed as part of the AOCI spectrometer upgrade. When used with the 10 bit boards, the interconnect card re-routes the least significant two bits from each of the four infrared channel data streams and combines them into an 8 bit value for output as channel 1 data. In post processing, the 10 bit values can be reconstructed and used to more precisely define the calibration values and scene temperature variations. The associated improvement in truncation error and instrument sensitivity is discussed in the next section.

Figures 2 - 4 present calibration information for the 11 and 12 micrometer bands of MAMS for three observation periods. These calibration values represent instrument performance in three different configurations. Channel 11 corresponds to the "cleanest" band while channel 12 is the "noisiest" of the four bands. The 1985 plots (Fig. 2a, 2b) represent the data quality discussed in the previous report. It is apparent that significant variations in the blackbody counts occur without a corresponding change in the temperature of the blackbodies, particularly in channel 12. This is believed to be the result of the DC restoration discussed below and the sensitivity of this channel to noise. Figure 2b presents the same calibration values after being filtered with a 31 line running average. Note that many high frequency components in channel 12 have been removed but the long term trend remains. This multiple line average tends to suppress line-to-line variations in the calibrated scene data, thus reducing the noise and increasing the utility of the image data.

The calibration plots for 1986 data (Fig. 3a, 3b) represent scan speed, aperture, and blackbody sampling changes of the instrument. The low frequency fluctuations apparent in Fig. 3a have been greatly suppressed by the instrument changes. High frequency components with amplitudes of 3-4 counts still exist, however. Filtering as in the previous example but over a smaller window (9 lines) serves to significantly improve the blackbody

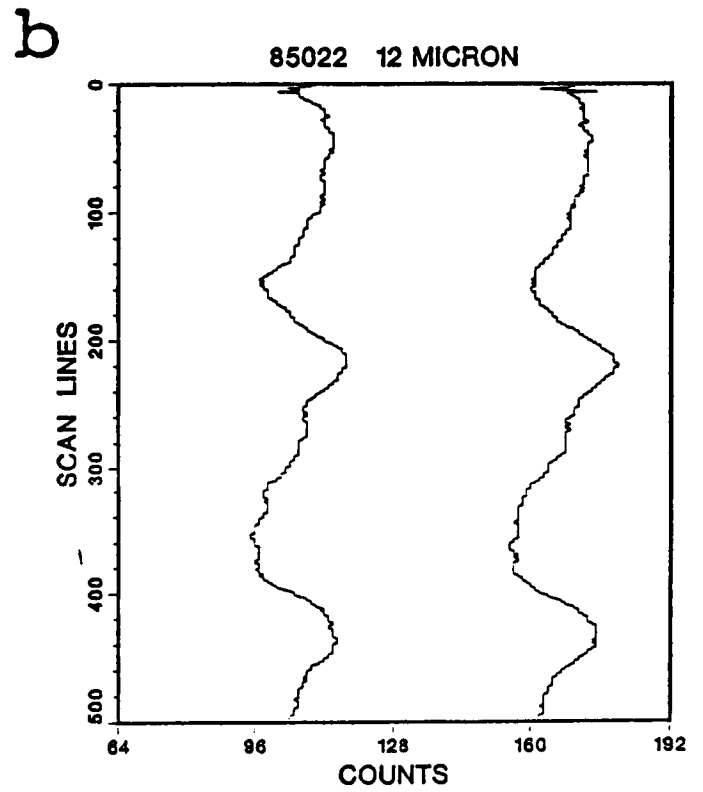
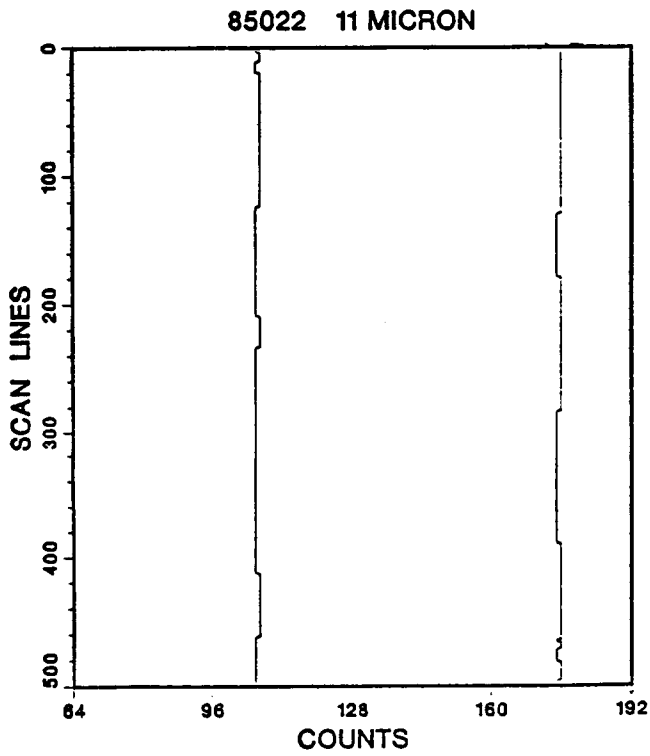
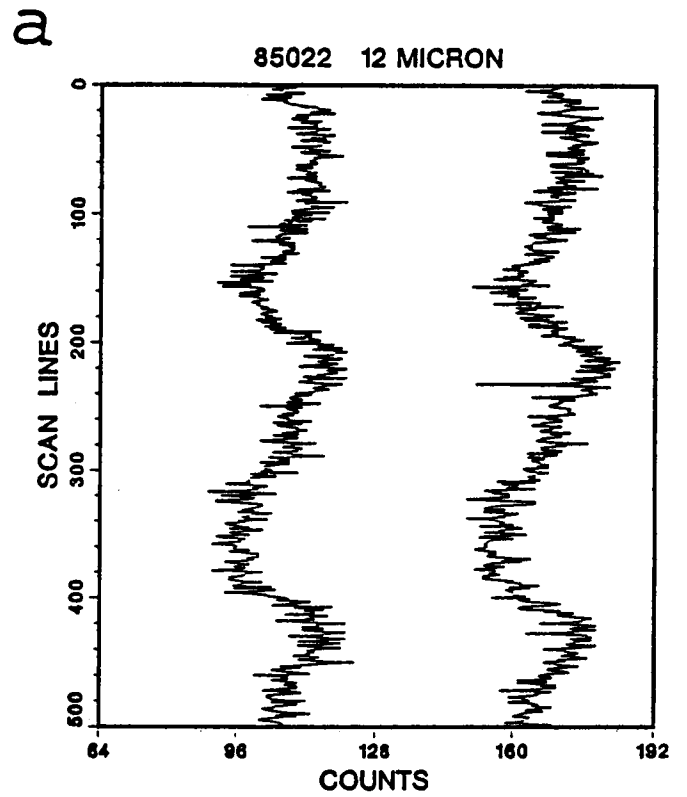
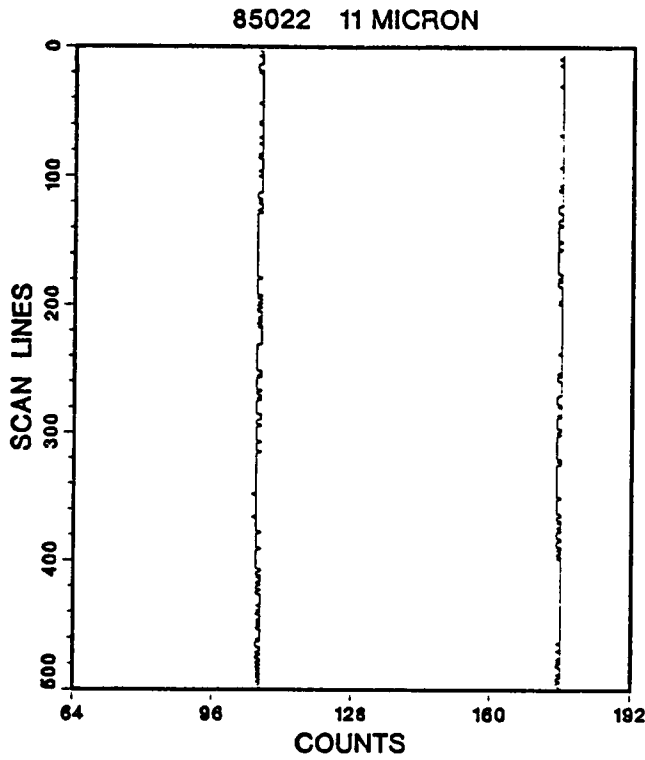


Figure 2. Channel calibration data representative of the 1985 instrument configuration. The upper diagrams (a) present unsmoothed data while the lower pair (b) have been filtered.

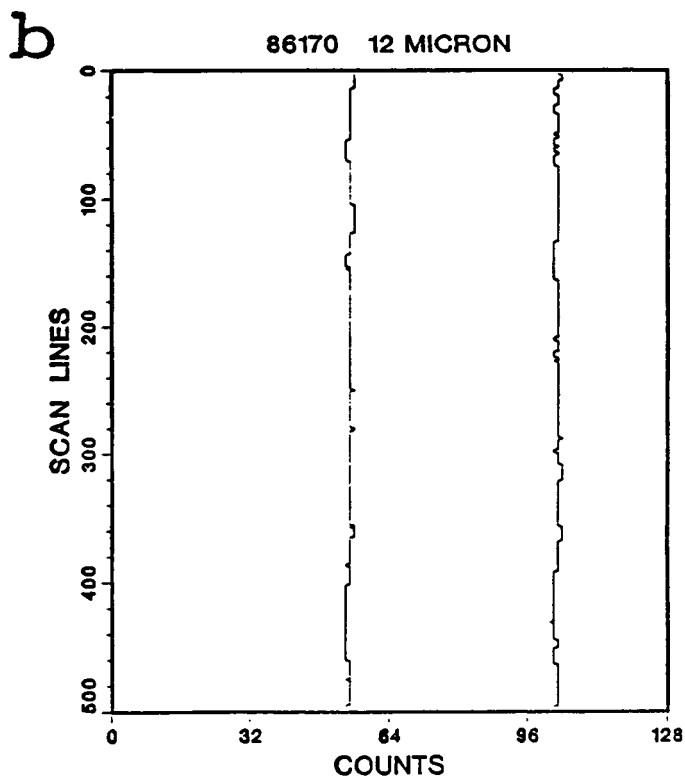
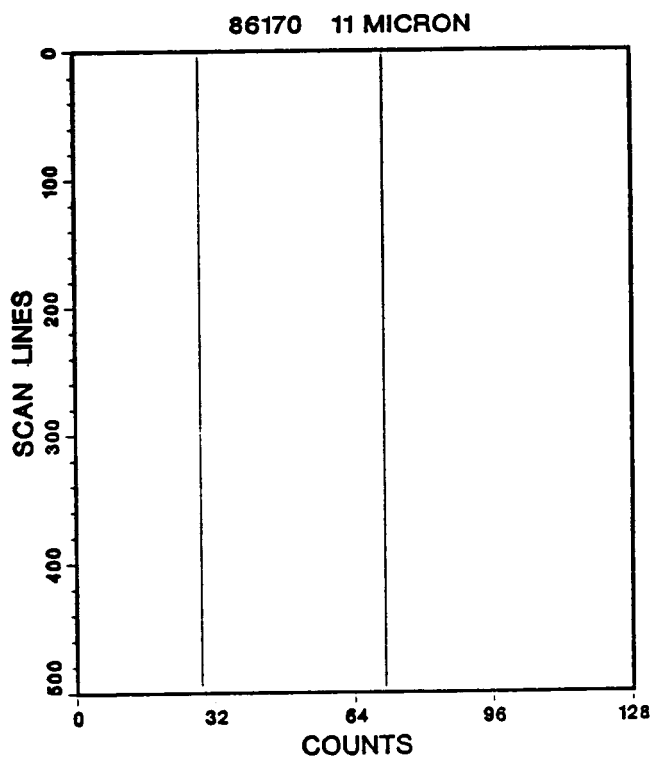
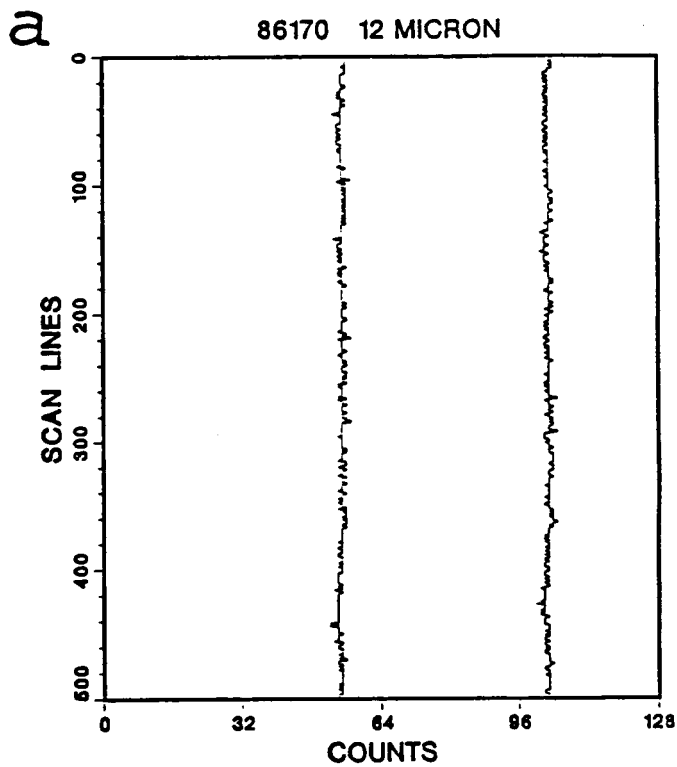
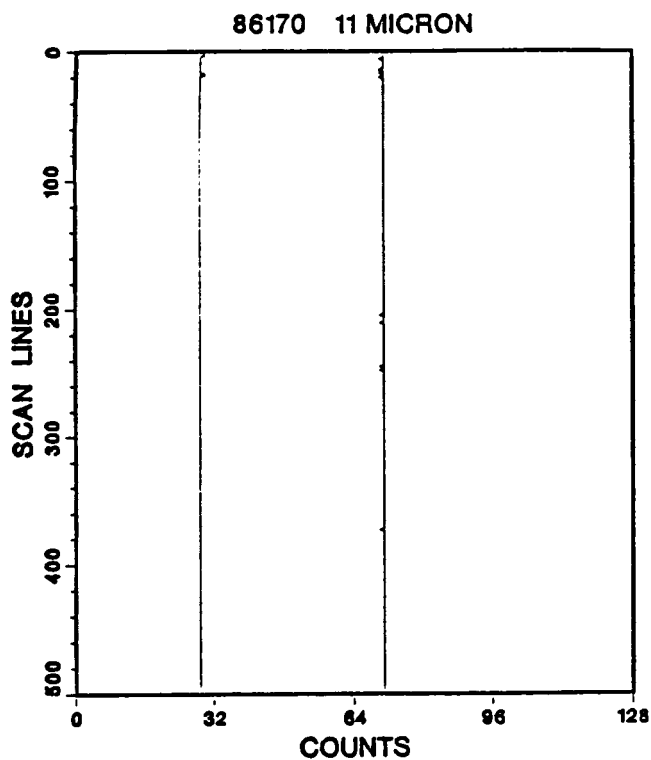


Figure 3. Channel calibration data representative of the COHMEX instrument configuration of 1986. The upper diagrams (a) present unsmoothed data while the lower pair (b) have been filtered.

count values (Fig. 3b). It will be shown later that the reduction in this count value noise considerably improves the quality of the calibrated data.

The calibration plots for 1987 data (Fig. 4a, 4b) represent the current and most improved instrument configuration (full aperture scan mirror and 10 bit quantization). In Fig 4a, the 8 bit calibration values for both channels exhibit only small fluctuations. Little filtering is necessary or even helpful. These fluctuations, which are 1 - 2 count values in amplitude, are mainly due to truncation by the 8 bit conversion. Although these fluctuations are small they correspond to 0.3 - 0.5 Kelvin fluctuations in the scene data. Figure 4b presents the same calibration data but after 10 bit values have been reconstructed. While more variations are apparent in the 10 bit values, each count represents one-fourth of an 8 bit value and corresponds to more consistent variations sensed by the detectors. These 10 bit values increase the sensitivity and accuracy of the calibrated scene data.

Based on the current instrument performance, minimal changes are necessary for the collection of high quality data in the future. As noted above, however, low frequency variations in the blackbody counts are still apparent. This is thought to be due to either instabilities in the pre-amplifiers or improper DC restoration. DC restoration is an approach used to correct the IR detector output for DC component variations which are not attributed to the scene. Two levels of DC restoration exist in the MAMS scanner system and act on every scanline of data: a long term integration circuit (10 seconds) and a short term circuit. The long time integration circuit compensates for scan head temperature variations and also keeps the pre-amplifiers from saturation. An operational amplifier is used in an integrator configuration to sense the average DC level of the detector output. This average taken over a complete revolution of the scan mirror and over multiple revolutions becomes an error signal which is fed back to the pre-amplifiers to force an average zero DC output. The 10 second time constant of the integrator will give less than a 1% change per scan line at 6.25 rps for a step function change lasting for one field of view. Thus, this circuit has little response to small scene changes and responds mainly to housing temperature variations. However, if the scene temperature changes dramatically (e.g., from a warm surface to a cold thunderstorm top) over a ten second period, the scene induced temperature variations will force a change in the zero DC output value and create count value variations unrelated to scan head temperature changes.

The short term correction circuit uses both blackbodies in the DC restoration process for the infrared channels. This circuit was added in the original Daedalus configuration to help offset detector variations related to drift on a shorter time

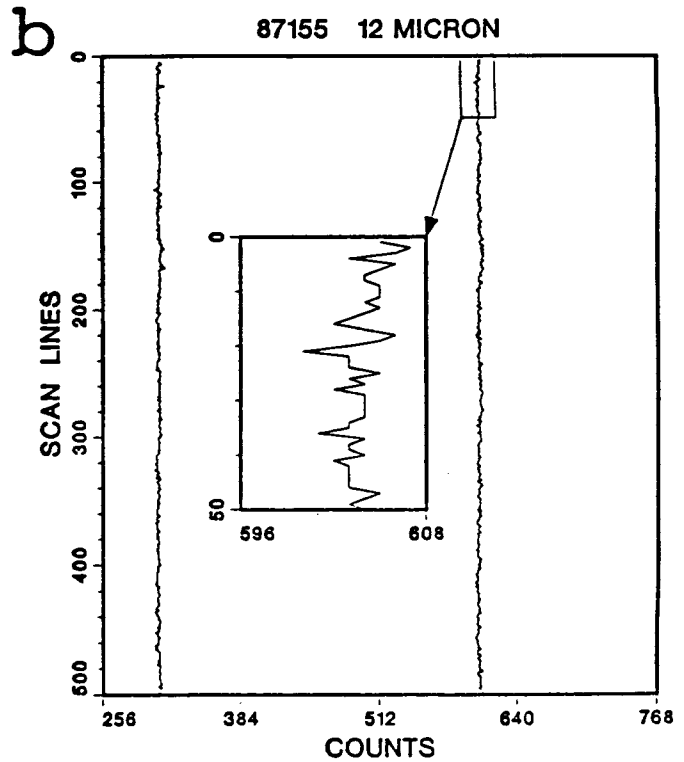
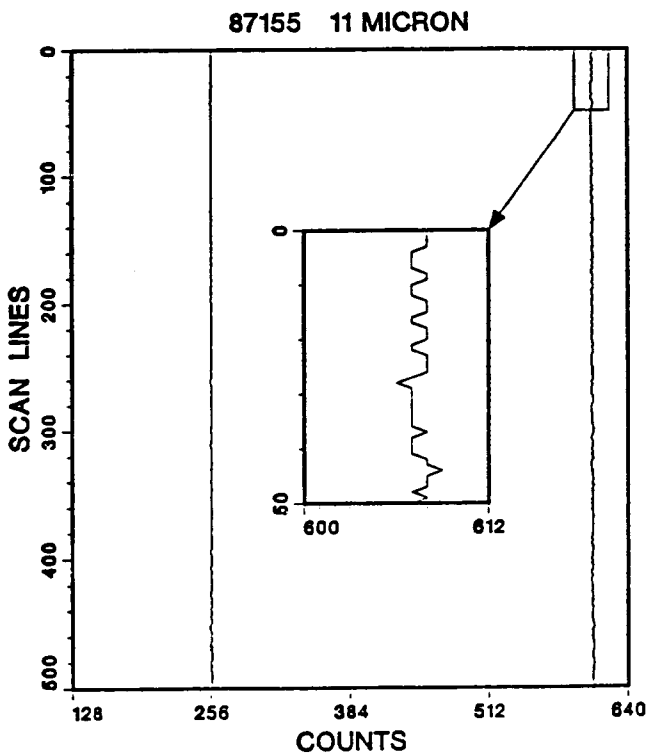
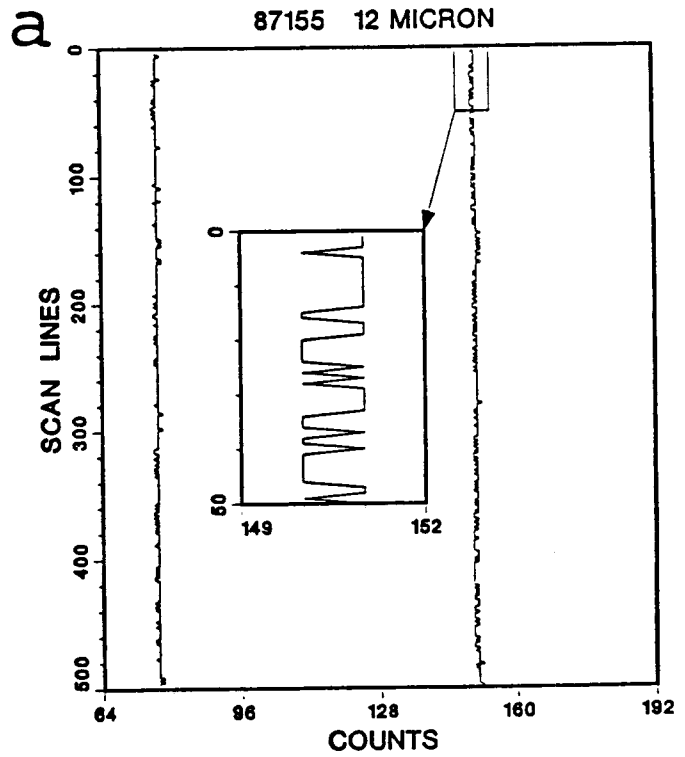
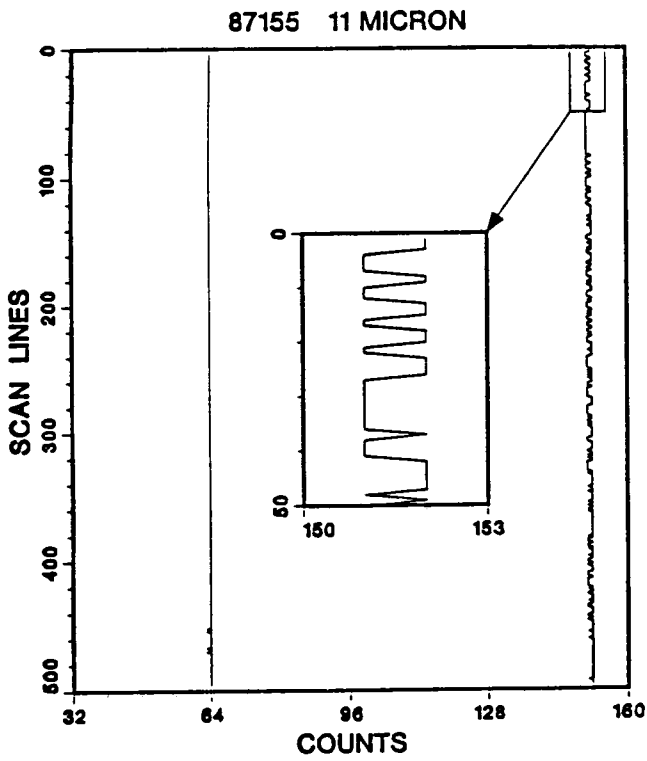


Figure 4. Channel calibration data representative of the 1987/1988 and current instrument configuration. The upper diagrams (a) present 8 bit data while the lower pair (b) present the same calibration information at 10 bit resolution.

interval. During one revolution of the scan mirror each blackbody is scanned and multiple blackbody samples are time averaged. When one of the blackbodies is not controlled, low frequency variations in blackbody readings are observed. Tests are planned with changed DC restoration circuitry such that all values are restored to a constant signal.

Capabilities to measure energy in other regions of the infrared spectrum are currently being investigated. Other possible bandpass filters must be compatible with the dichroic filters. In September 1986, an additional dewar/ detector/ filter/ pre-amplifier combination was obtained for the MAMS (see Table 3 and Fig. 5). The new channel is similar to the 3.7 micrometer channel of the AVHRR. Because of the spectral characteristics of the first and second dichroic filters (see Jedlovec et al., 1986a), the new channel can only be used in place of the 6.5 micrometer channel. Interchangeable channels, such as the 6.5/ 3.7 micrometer channels, will provide underflight capabilities with other current satellite sensors and with planned Eos instrumentation in the 1990's.

-----

Table 3

Infrared channel spectral characteristics. Only three independent bands are available at one time and the 6.54 and 3.73 bands can not be used together.

| Channel | Central Wavelength<br>(micrometers) | Bandwidth (@50% response)<br>(micrometers) |
|---------|-------------------------------------|--|
| 9       | 3.73                                | 3.47 - 3.86                                |
| 10      | 6.54                                | 6.28 - 6.98                                |
| 11      | 11.12                               | 10.55 - 12.24                              |
| 12      | 12.56                               | 12.32 - 12.71                              |

-----

The results of the instrument improvements discussed in this section can be viewed in Figures 6, 7, and 8. These figures show the images for the three infrared spectral channels on the MAMS flight of 27 January 1988. Note the good quality of the imagery (especially in the previously noisy 12.5 micrometer band) and the significantly improved quality compared to that presented in the previous report. The lack of line-to-line variations allow for an accurate interpretation of fine scale horizontal thermal variations. The next section discusses the quantitative calibration of these radiances.

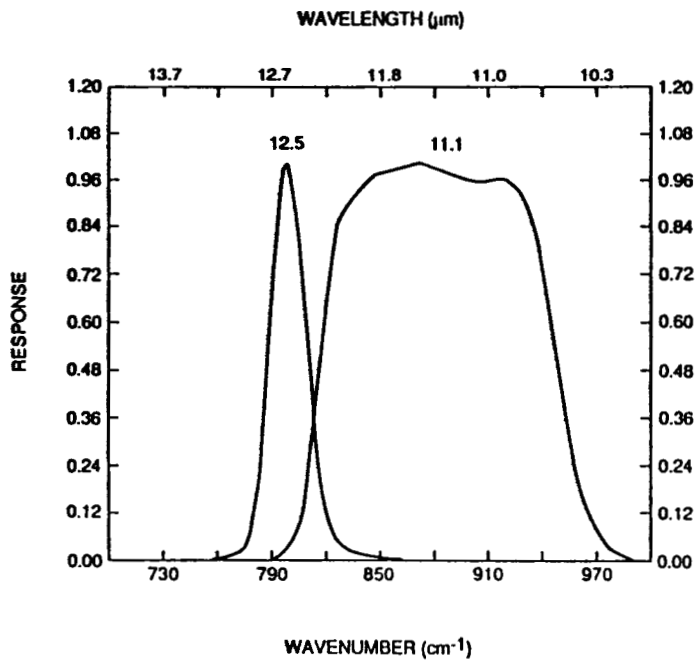
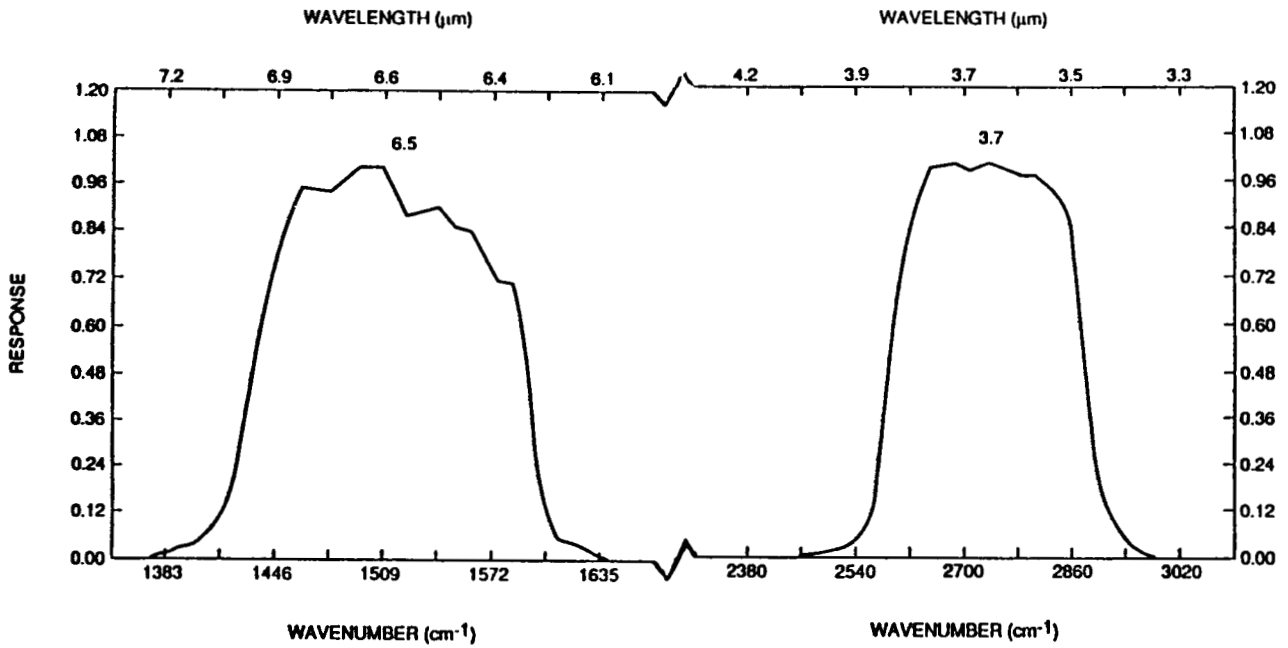


Figure 5. Spectral response curves for the four infrared channels of MAMS. The vertical axis indicates the magnitude of the response for each wavelength or wavenumber indicated on the horizontal axes. Note the discontinuity in the axis between the 3.7 and 6.5 micrometer channels.

ORIGINAL PAGE IS  
OF POOR QUALITY



Figure 6. MAMS 3.7 micrometer calibrated image for 27 January 1988 off the coast of Louisiana. The image is enhanced to bring out subtle thermal variations in the scene. Dark grey-shades indicate relatively warm features and light grey-shades colder features.

ORIGINAL PAGE IS  
OF POOR QUALITY



Figure 7. MAMS 11.1 micrometer calibrated image for 27 January 1988 off the coast of Louisiana. Note the total lack of line-to-line variations, indicating the excellent relative accuracy of this data. See caption on Fig. 6 for further description.

ORIGINAL PAGE IS  
OF POOR QUALITY



Figure 8. MAMS 12.5 micrometer calibrated image for 27 January 1988 off the coast of Louisiana. The lack of significant atmospheric water vapor and the good data quality allows the mapping of surface thermal features as with the 11 micrometer channel. See caption on Fig. 6 for further description.

### III. CALIBRATION

Both the visible and the infrared channels of the MAMS require post processing to convert raw counts into radiance values. Visible and infrared calibration is handled separately. Both procedures are discussed below.

#### A. Visible Channel Calibration

In the MAMS configuration, in-flight calibration data are not available for the visible channels. Raw data in the visible channels are converted to radiance units based on pre/post-flight calibration data with a known light source. In the laboratory, the MAMS is operated while viewing a constant light source from an integrating sphere. The intensity of the light from the sphere is accurately known in 10 nm increments throughout the visible and near infrared portion of the spectrum. The integrating sphere itself is calibrated periodically against Bureau of Standards precision instrumentation. The relationship of the observed versus known intensity values is modeled based upon the spectral response characteristics of the MAMS visible channels. The resultant calibration values are used to convert flight data to radiance units in a multiplicative way. These visible channel calibration values are presented in Tables B1 through B4 of Appendix B for a number of MAMS flights.

The visible channel calibration values can change from one flight to another for a number of reasons. First, the calibration values are based on the channel gain values. As these gain values are changed, the channel sensitivity changes and therefore new calibration values are necessary. Second, since the values are based on the throughput of the entire optical system, instrument degradation (as a function of time) may have an effect on the calibration. Third, haze and particulate build-up on the scan mirror itself may affect the signal. Since the scan mirror is exposed to the elements throughout the flight, haze, atmospheric pollution, and water vapor contribute to the build up of a film on the scan mirror. This film affects the longer visible channel wavelengths most. It is not advisable to clean the scan mirror too often since this will remove the mirror coating and change its reflection properties at all wavelengths. Thus as the film builds up (which is often undetected by the naked eye), the throughput of the instrument is reduced. In other instrument configurations, the effect of this film build-up has reduced the intensity in several of the channels by up to 15% (personal communication, Jeff Myers, NASA Ames Research Center). Therefore, in order to obtain accurate visible channel data, periodic calibration with the integrating sphere is recommended.

## B. Infrared Channel Calibration

The current infrared calibration procedure is similar to that presented in the previous report. The MAMS views a warm and a cold blackbody of known temperature every spin (6.25 times per second in the standard configuration). Because of the instrument modifications discussed in Section II, the calibration values in each infrared channel are much more reliable than previously reported and multiple line averaging is usually not necessary (see Fig. 4).

The upwelling radiance,  $R$ , determined by MAMS in a particular channel,  $i$ , from a scene with observed temperature,  $T$ , is given by the convolution of the channel spectral response  $SR_i(\nu)$  and the Planck radiance  $\beta(T, \nu)$  as

$$R_i(T) = \frac{\int_0^{\infty} \beta(T, \nu) SR_i(\nu) d\nu}{\int_0^{\infty} SR_i(\nu) d\nu} \quad (4)$$

where  $\nu$  represents the wavenumber domain. The spectral response curves for the four MAMS channels were given in Fig. 5. For easier radiance determinations, (4) is often approximated by

$$R_i(T) = \beta(T, \nu_0) \quad (5)$$

where  $\nu_0$  is the half power wavenumber defined by

$$\nu_0 \equiv \frac{\int_0^{\nu_0} SR(\nu) d\nu}{\int_0^{\infty} SR(\nu) d\nu} = 0.50 \quad (6)$$

This half power wavenumber best represents the asymmetric characteristics of the spectral response curve (Fig. 5). When  $\nu_0$  is used in (5), the Planck function ( $\beta$ ) approximates the energy in a MAMS channel for a given scene temperature ( $T$ ). Since the Planck function peak (maximum emission) shifts (with respect to wavelength or wavenumber) with changing scene temperature, a correction to the half power wavenumber is necessary. This monochromaticity correction is more conveniently applied to the temperature in (5) than to the wavenumber and is calculated by forming linear relationships between  $\nu_0$  and  $T$  over a typical range of scene temperatures. This application produces corrections in each channel given by

$$T_c = (T - a_2) / a_1 \quad (7a)$$

so that an improved expression becomes

$$R_V(T) = \beta(T_c, V_0) \quad (7b)$$

where  $a_1$  and  $a_2$  are linear regression coefficients. Values for the half power wavenumbers and the temperature correction coefficients are listed in Table 4. Equation (7) is only used in the calibration equations presented below; otherwise, the more rigorous equation (4) is used.

Table 4

Half power wavenumbers and monochromaticity corrections for MAMS infrared channels. See text for explanation of the coefficients ( $a_1$ ) and ( $a_2$ ).

| Half Power Wavelength (micrometers) | Half Power Wavenumber ( $\text{cm}^{-1}$ ) | $a_1$      | $a_2$ (Kelvins) |
|-------------------------------------|--|------------|-----------------|
| 3.65                                | 2739.654                                   | 1.00292492 | -2.12060547     |
| 6.62                                | 1510.429                                   | 1.00285721 | -1.06420898     |
| 11.30                               | 885.020                                    | 1.00362206 | -0.99682617     |
| 12.48                               | 801.589                                    | 1.00067425 | -0.18969726     |

Prior to each flight, the gain and offset for each infrared channel are set to optimize channel sensitivity and dynamic range for a particular flight. Likewise, the blackbody temperatures are selected to encompass the expected scene temperatures. (It should be noted that while the blackbody temperatures are electronically controlled, at flight altitude the cold blackbody can not be held at a temperature cooler than about 245 Kelvin). The analog to digital processing of the MAMS data during flight converts the DC restored channel voltages into 8 (or 10) bit raw count values. These raw values are related to the energy received by the detectors in both the scene and blackbody values through an assumed linear response given by

$$R_i = b_i + m_i * C_i \quad (8)$$

where  $R$  is the calculated radiance,  $C$ , the raw count value, and the subscript,  $i$ , the channel designator. Jedlovec et al. (1986a) reported the fractional non-linearity to be on the order of  $10^{-4}$ . Thus, the blackbody radiances,  $R_i$ , (via equation (8)) and the corresponding channel counts,  $C_i$ , form calibration curves for MAMS infrared channels. Values  $m$  and  $b$  are the slope and

intercept for the i-th channel and are given by

$$b_i = \frac{(C_{ci} R_{hi} - C_{hi} R_{ci})}{(C_{ci} - C_{hi})} \quad (9)$$

$$m_i = \frac{(R_{hi} - R_{ci})}{(C_{hi} - C_{ci})} \quad (10)$$

where the subscripts h and c denote the hot and cold blackbodies, respectively. An example of a calibration curve for each of the four infrared channels is presented in Fig. 9 based on a single scan line of data. Numerical values are presented in Table 5.

In Table 5, column 1 represents the configuration channel number for each of the four infrared bands, column 2 the respective wavenumber for each band (from equation (6)), and columns 3 and 4 the channel values when viewing the cold and warm blackbodies, respectively. Columns 5 and 6 represent the channel radiances for each blackbody (based on (7)). The slope (m) and intercept (b) for the lines in Fig. 9 are given in columns 7 and 8. These values are used to calibrate scene data over each scan line and are recomputed for each scan line to incorporate blackbody temperature and DC restoration changes. The maximum and minimum temperatures measurable in each channel are presented in the last two columns of Table 5.

The slope value (m in column 7) actually is a measure of the channel sensitivity and can be inferred from Fig. 9. The sensitivity is a function of temperature and therefore inverse equations to (7a) and (7b) are used to convert radiance to temperature. Sensitivity values (counts/Kelvin) for 8 and 10 bit data are presented in Table 6 for selected scene temperatures. It is apparent that the sensitivity decreases with temperature for all channels. For the earth viewing channels (3, 11, and 12 micrometers), typical scene temperatures may vary from 275 to 325 Kelvins. Corresponding 8 bit channel sensitivities range from 2.50 to 3.70 counts/Kelvins for the 11 and 12 micrometer channels and from 0.90 to 5.88 counts/Kelvins for the 3 micrometer channel. For cloudy scenes, sensitivity to changes in cloud top temperature decreases rapidly as the temperature drops below 225 Kelvin. Thus, the determination of both relative and absolute cloud top temperature is less certain for cold cloud features. For the atmospheric water vapor channel, scene temperatures vary from 225 to 275 Kelvins with channel sensitivities from 2.22 to 8.33 counts/Kelvins, respectively.

-----

Table 5

Infrared channel calibration information used in Figure 9 for normal gain and offset settings. Values are presented for both 8 (A) and 10 (B) bit data. Data for channels 9, 11, and 12 are from the 15 January 1988 test flight and channel 10 from 7 June 1987 science flight.

(A)

| Channel | Halfpower Wavenumber (cm <sup>-1</sup> ) | C <sub>c</sub> | C <sub>h</sub> | R <sub>c</sub>                                    | R <sub>h</sub> | m     | b      | T <sub>max</sub> | T <sub>min</sub> |
|---------|--|----------------|----------------|---|----------------|-------|--------|------------------|------------------|
|         |  |                |                | (erg/(s-ster-cm <sup>2</sup> -cm <sup>-1</sup> )) |                |       |        | (Kelvin)         |                  |
| 9       | 2739                                     | 25             | 61             | .07   | .38            | .0086 | -.143  | 337.9            | 0.0              |
| 10      | 1510                                     | 171            | 246            | 9.47  | 13.48          | .0535 | .325   | 272.1            | 185.0            |
| 11      | 885                                      | 67             | 152            | 64.28   | 111.03         | .5503 | 27.433 | 325.1            | 223.0            |
| 12      | 802                                      | 75             | 162            | 75.83   | 124.77         | .5629 | 33.632 | 322.8            | 221.3            |

(B)

| Channel | Halfpower Wavenumber (cm <sup>-1</sup> ) | C <sub>c</sub> | C <sub>h</sub> | R <sub>c</sub>                                    | R <sub>h</sub> | m     | b      | T <sub>max</sub> | T <sub>min</sub> |
|---------|--|----------------|----------------|---|----------------|-------|--------|------------------|------------------|
|         |  |                |                | (erg/(s-ster-cm <sup>2</sup> -cm <sup>-1</sup> )) |                |       |        | (Kelvin)         |                  |
| 9       | 2739                                     | 100            | 247            | .07   | .38            | .0021 | -.139  | 336.5            | 0.0              |
| 10      | 1510                                     | 686            | 984            | 9.47  | 13.48          | .0135 | .237   | 272.2            | 180.1            |
| 11      | 885                                      | 268            | 608            | 64.28   | 111.03         | .1375 | 27.433 | 325.3            | 223.0            |
| 12      | 802                                      | 303            | 648            | 75.83   | 124.77         | .1419 | 32.840 | 323.2            | 220.3            |

-----

Using identical channel gain and offset settings, 10 bit digitization provides much greater sensitivities to scene temperature variations at all temperatures and channels as seen in the lower half of Table 6. For the most part these sensitivity values increase by a factor of four with the 10 bit data. It should be noted that both the scene data and the calibration data have this increased sensitivity which leads to substantially improved calibration, particularly at cold and warm temperatures (discussed below).

Data errors can be either random or systematic and can arise from a number of sources. Random error is usually the easiest to handle because simple averaging can considerably reduce the effects of this noise. Random and systematic noise are often masked by truncation error (the level of quantization). Table 7 presents the maximum possible error in calibrated MAMS data based

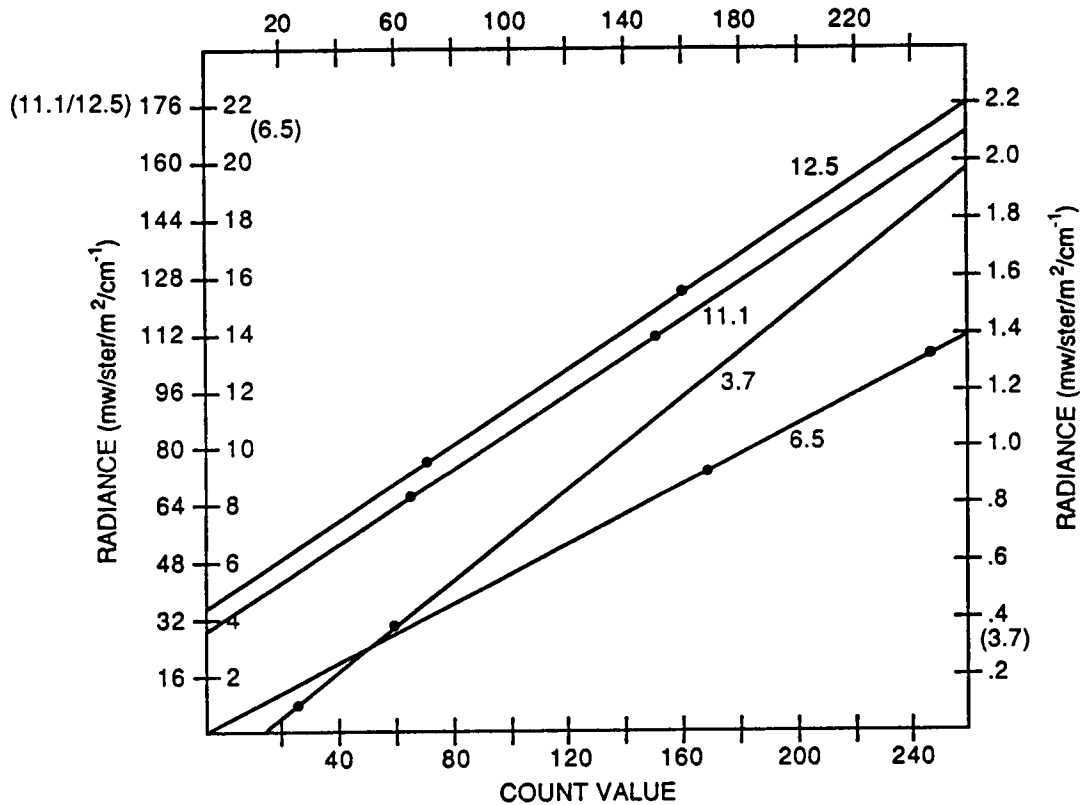


Figure 9. Typical calibration curves for the four MAMS infrared channels. These lines pictorially represent the data presented in Table 5. The outer left axis labels are used for the 11.1 and 12.5 micrometer channels, the inner labels for the 6.5 micrometer channel, and the right outer labels for the 3.7 micrometer channel.

only on truncation error in the blackbody count values. Values are in Kelvins for each channel based on typical 8 and 10 bit instrument configurations (see Table 5). Calibration value truncation error leads to larger scene data errors when extrapolation is used for scene values colder or warmer than the blackbodies. Truncation error also depends on the channel sensitivity at the blackbody temperatures. The effects can be seen in Table 7 at cold temperatures where sensitivity is poor and extrapolation away from the blackbody values is needed to calibrate the data. For temperatures near that of the blackbodies, the truncation error is relatively small. Typical values in this range are generally less than 0.50 Kelvins for 8 bit digitization. For warm scenes where sensitivity is good but extrapolation is need, truncation error slightly increases. With 10 bit data, the effect of blackbody truncation error is

-----

Table 6

Channel sensitivities (counts/Kelvins) for 8 (A) and 10 (B) bit data and calibration values in Table 5.

(A)

8 Bit Sensitivity (counts/Kelvins)

| Band | Scene Temperatures (Kelvins) |      |      |      |      |      |
|------|------------------------------|------|------|------|------|------|
|      | 200                          | 225  | 250  | 275  | 300  | 325  |
| 3.7  | .00                          | .05  | .27  | .90  | 2.44 | 5.88 |
| 6.5  | .67                          | 2.22 | 5.00 | 8.33 | -    | -    |
| 11.1 | .95                          | 1.33 | 1.89 | 2.50 | 3.13 | 3.70 |
| 12.5 | 1.05                         | 1.47 | 2.04 | 2.56 | 3.13 | 3.57 |

(B)

10 Bit Sensitivity (counts/Kelvins)

| Band | Scene Temperatures (Kelvins) |      |       |       |       |       |
|------|------------------------------|------|-------|-------|-------|-------|
|      | 200                          | 225  | 250   | 275   | 300   | 325   |
| 3.7  | .00                          | .19  | 1.04  | 3.57  | 5.00  | 25.00 |
| 6.5  | 3.13                         | 8.33 | 16.67 | 25.00 | 33.33 | 50.00 |
| 11.1 | 3.80                         | 5.26 | 7.69  | 10.00 | 12.50 | 14.29 |
| 12.5 | 4.21                         | 5.88 | 8.33  | 10.00 | 12.50 | 16.67 |

-----

minimized over a wider range of scene temperatures. This occurs because errors are reduced by roughly a factor of four when 10 bit digitization is used for the same instrument gains.

Truncation error also occurs in digitizing the scene data as well. These errors are only a function of channel sensitivity at the scene temperature and are presented in Table 8. Errors show a different trend than those in Table 7 since they only depend on sensitivity (a function of channel and temperature). Errors for all channels decrease at warmer temperatures. With 10 bit digitization, the effect of this error is negligible for the 3 micrometer channel at scene temperatures less than 275 Kelvin, and for the other channels at scene temperatures of 200 Kelvin or less.

-----

Table 7

Maximum error in scene data due to truncation of the calibration count values. Values are based on a typical MAMS configuration presented in Table 5 for both 8 and 10 bit data. Values are in Kelvins. See text for further discussion.

Maximum Error from Calibration Value Truncation

| 8 bit  |      |       |      |     |     |      |
|--------|------|-------|------|-----|-----|------|
| Band   | 200  | 225   | 250  | 275 | 300 | 325  |
| 3.7    | -    | 12.85 | 4.63 | .65 | .66 | 1.33 |
| 6.5    | 5.60 | 1.96  | .05  | .23 | -   | -    |
| 11.1   | 3.58 | 1.81  | .80  | .18 | .42 | .89  |
| 12.5   | 3.23 | 1.69  | .22  | .07 | .54 | .95  |
| 10 bit |      |       |      |     |     |      |
| Band   | 200  | 225   | 250  | 275 | 300 | 325  |
| 3.7    | -    | 5.08  | 1.21 | .16 | .16 | .30  |
| 6.5    | 1.60 | .50   | .11  | .08 | -   | -    |
| 11.1   | .94  | .47   | .21  | .03 | .11 | .25  |
| 12.5   | .83  | .44   | .17  | .03 | .12 | .22  |

-----

The combined maximum truncation error in calibrated MAMS scene data (due to the two sources discussed above) is presented in Table 9. For typical scene temperatures, maximum truncation errors range from 0.27 - 0.74 Kelvins for the 6, 11, and 12 micrometer channels, and 0.94 - 1.75 Kelvins for the 3 micrometer channel with 8 bit data. For data collected with 10 bit digitization, these errors are substantially reduced to less than 0.2 Kelvins for the 6, 11, and 12 micrometer channels and less than 0.4 Kelvins for the 3 micrometer channel. It should be noted that these values (Tables 7 - 9) represent the maximum possible truncation error. Typically, truncation error will not be this severe and is nominally one half (or less) of that presented in Table 9. Therefore, the effects of truncation error are negligible for typical scene temperatures. For non-typical scenes (e.g., cold cloud tops), truncation error is not negligible and Table 9 can be used to define the upper bounds in truncation error.

-----

Table 8

Maximum error in scene data due to truncation of the scene data itself. Values are based on a typical MAMS configuration presented in Table 5 for both 8 and 10 bit configurations. Values are in Kelvins. See text for further discussion.

Maximum Error from Scene Value Truncation

8 bit

| Band | 200  | 225   | 250  | 275  | 300 | 325 |
|------|------|-------|------|------|-----|-----|
| 3.7  | -    | 12.92 | 3.34 | 1.10 | .28 | .18 |
| 6.5  | 1.00 | .46   | .22  | .12  | -   | -   |
| 11.1 | 1.20 | .74   | .52  | .40  | .32 | .26 |
| 12.5 | 1.02 | .68   | .50  | .38  | .32 | .28 |

10 bit

| Band | 200 | 225  | 250 | 275 | 300 | 325 |
|------|-----|------|-----|-----|-----|-----|
| 3.7  | -   | 3.91 | .98 | .28 | .10 | .04 |
| 6.5  | .32 | .12  | .06 | .03 | -   | -   |
| 11.1 | .30 | .19  | .13 | .10 | .08 | .05 |
| 12.5 | .25 | .17  | .12 | .10 | .08 | .07 |

-----

C. Noise Estimates

Single sample noise is calculated two ways for MAMS infrared data. First, the single sample noise is estimated with the use of structure functions (Hillger and Vonder Haar, 1988, Jedlovec, 1987, and Hillger and Vonder Haar, 1979). This approach has a wide application since it does not require a perfectly uniform scene. Second, the variance is computed directly over a uniform scene to estimate the single sample noise in the radiance data. In the later case, a uniform water scene is usually required. Both approaches are used to demonstrate consistency in the error estimates. Single sample noise has not been estimated for the visible channels.

Tables 10 and 11 summarize the single sample noise estimates for several flights and different instrument configurations based on these two approaches. When available, noise estimates are presented for 10 bit data. Noise estimates for single and

-----

Table 9

Maximum error in scene data due to truncation error in both the scene and calibration data. These values are a combination of those in Tables 7 and 8. Values are presented in Kelvin for both 8 and 10 bit configurations.

Maximum Total Truncation Error

| 8 bit     |      |       |      |      |     |      |
|-----------|------|-------|------|------|-----|------|
| channel   | 200  | 225   | 250  | 275  | 300 | 325  |
| 9 (3.7)   | -    | 25.77 | 8.37 | 1.75 | .94 | 1.51 |
| 10 (6.5)  | 6.60 | 2.42  | .27  | .35  | -   | -    |
| 11 (11.1) | 4.78 | 2.55  | 1.32 | .58  | .74 | 1.15 |
| 12 (12.5) | 4.25 | 2.37  | .72  | .45  | .67 | 1.32 |
| 10 bit    |      |       |      |      |     |      |
| channel   | 200  | 225   | 250  | 275  | 300 | 325  |
| 9 (3.7)   | -    | 8.98  | 2.18 | .43  | .26 | .34  |
| 10 (6.5)  | 1.72 | .62   | .17  | .11  | -   | -    |
| 11 (11.1) | 1.24 | .66   | .34  | .13  | .19 | .30  |
| 12 (12.5) | 1.08 | .61   | .23  | .13  | .20 | .29  |

-----

multiple line averages are presented for 8 bit data (as in the previous study) when 10 bit data are not available. Table 10 presents the results from the structure function approach while Table 11 presents them for the variance method. In Table 10, noise estimates are presented based on extrapolation of structure results to zero separation distance for isotropic (ISO), along track (L), and across (C) track conditions. The first condition (ISO) considers gradient information in every direction in the imagery and calculates structure for every pair of points in the image. The latter conditions consider only unidirectional pixel pairings and can be used to isolate noise due to line-by-line calibration variations (L) and due to "true" single sample variability (C).

Case 1 presents the results from the earliest MAMS configuration used in 1985. Single sample noise results (variance method) were presented for this case in the previous report but were re-calculated and presented here for direct

Table 10

Single sample noise calculations based on spatial structure for six different MAMS flights. The different flights represent various instrument configurations over the past three years. Values were determined by extrapolating structure curves to zero separation distance. "Iso" denotes isotropic structure calculations, while "L" and "C" denote along track and across track calculations, respectively. All units are in Kelvins. See text for further details.

Case 1: 22 Jan 85 (8 bit)

| Channel | Band | Scene Temp | w/o avg |      |      | 31 line avg |      |      |
|---------|------|------------|---------|------|------|-------------|------|------|
|         |      |            | Iso.    | L    | C    | Iso.        | L    | C    |
| 9       | 6.5  | 244        | .62     | .71  | .42  | .54         | .60  | .43  |
| 10      | 6.5  | 244        | .67     | .73  | .50  | .61         | .43  | .50  |
| 11      | 11.1 | 278        | .21     | .24  | .14  | .20         | .21  | .14  |
| 12      | 12.5 | 278        | 3.78    | 4.51 | 2.06 | 2.18        | 2.32 | 2.00 |

Case 2: 5 July 86 (8 bit)

| Channel | Band | Scene Temp | w/o avg |      |      | 31 line avg |      |      |
|---------|------|------------|---------|------|------|-------------|------|------|
|         |      |            | Iso.    | L    | C    | Iso.        | L    | C    |
| 9       | 6.5  | 236        | .28     | .29  | .07  | .18         | .24  | .07  |
| 10      | 11.1 | 287        | .08     | .11  | <.05 | <.05        | <.05 | <.05 |
| 11      | 11.1 | 287        | <.05    | <.05 | <.05 | <.05        | <.05 | <.05 |
| 12      | 12.5 | 282        | .32     | .45  | <.05 | .34         | .49  | <.05 |

Case 3: 29 May 87 (8 bit)

| Channel | Band | Scene Temp | w/o avg |     |      | 31 line avg |     |     |
|---------|------|------------|---------|-----|------|-------------|-----|-----|
|         |      |            | Iso.    | L   | C    | Iso.        | L   | C   |
| 9       | 3.7  | 291        | .49     | .62 | <.05 | .49         | .61 | .07 |
| 10      | 3.7  | 291        | .47     | .58 | .07  | .47         | .57 | .07 |
| 11      | 11.1 | 292        | .07     | .07 | .07  | .07         | .07 | .07 |
| 12      | 12.5 | 289        | .21     | .29 | .12  | .20         | .23 | .12 |

Table 10 (continued)

Case 4: 4 June 1987

| Channel | Band | Scene Temp | 10 bit data |     |     |
|---------|------|------------|-------------|-----|-----|
|         |      |            | Iso.        | L   | C   |
| 9       | 3.7  | 296        | .35         | .34 | .23 |
| 10      | 3.7  | 296        | .52         | .46 | .37 |
| 11      | 11.1 | 297        | .28         | .28 | .22 |
| 12      | 12.5 | 292        | .17         | .17 | .17 |

Note: Some temperature gradient was apparent across scene

Case 5: 7 June 87

| Channel | Band | Scene Temp | 10 bit data |     |      |
|---------|------|------------|-------------|-----|------|
|         |      |            | Iso.        | L   | C    |
| 9       | 6.5  | 238        | .12         | .16 | .07  |
| 10      | 6.5  | 239        | <.05        | .07 | <.05 |
| 11      | 11.1 | 297        | <.05        | .10 | <.05 |
| 12      | 12.5 | 292        | .19         | .21 | .10  |

Case 6: 27 Jan 88

| Channel | Band | Scene Temp | 10 bit data |      |      |
|---------|------|------------|-------------|------|------|
|         |      |            | Iso.        | L    | C    |
| 9       | 3.7  | 284        | .28         | .35  | .10  |
| 10      | 3.7  | 283        | .23         | .24  | .14  |
| 11      | 11.1 | 284        | <.05        | <.05 | <.05 |
| 12      | 12.5 | 282        | .12         | .19  | .10  |

-----

comparison to later configurations. The single sample noise is quite large for this data, especially in the narrow 12.5 micrometer channel. This occurs because of the relatively low signal-to-noise provided by this instrument configuration. The large isotropic values are dominated by the along track noise which is considerably larger than the across track noise. This result indicates that line-to-line variations due to calibration errors are significant as was evident in Figs. 2a and 2b. When the calibration values are filtered (over 31 points) to reduce

the noise, the along track values are more similar to the across track ones. Even after filtering, noise values are rather high in the 12 micrometer channel. The 6 and 11 micrometer channel noise values are quite good for this early configuration. These structure function noise estimates are consistent with those from the variance approach presented in Table 11 and those listed in the previous report. The single sample noise estimates in Table 11 should be compared with the isotropic values in Table 10. Both sets of values show similar tendencies with the variance method producing slightly larger error estimates. This is expected if the scene contains any real gradient information.

Case 2 in Table 10 and 11 presents the results from a flight on 5 July 1986. This flight took place during the COHMEX (Arnold, 1986) over Tennessee and Alabama, and represents data collected with the larger aperture and slower scan speed previously discussed. Structure function noise estimates for these data are quite good: all values are less than 0.50 Kelvins. Since these channels have a sensitivity of around 3.0 counts/Kelvin, the noise estimates are smaller than the digitization error. This indicates that the instrument is outperforming the digitization of the data, and that improvements to the precision of the data will yield additional real scene variability. Across track noise estimates are extremely low because of the relatively high correlation from one pixel to the next along the scan line (Jedlovec et al, 1986). The variance method produces somewhat larger values, but shows a similar trend between channels and a reduction in noise with the averaging of calibration data.

Case 3 presents similar results but for data collected after the scanner was modified with the full aperture scan mirror. The 11 and 12 micrometer channels show noticeable reduction in noise in both the structure function and variance method estimates. Noise estimates for the 3.7 micrometer channel are significantly higher. This is not surprising since in this region of the Earth's energy spectrum, much less energy is emitted and detected by the sensor. This has the effect of decreasing the signal to noise ratio for the 3.7 micrometer channel data, thus resulting in higher noise estimates than those of the 11 and 12 micrometer channels.

The low noise values presented in Case 2 and 3 can be misleading if not properly analyzed. With channel sensitivity and truncation error at about 0.33 Kelvins/count (3.0 counts/Kelvin) fluctuations either real or due to noise are not always recorded in the digitized data. Thus, the configuration with the interconnect board and 10 bit digitizer cards used in the later flights can better address calibration and scene variations (both real and noise related). The increase in digitized variations due to noise now detected in the 10 bit data can be reduced with simple averaging methods without affecting

the real data trends.

Cases 4 - 6 in Table 10 present the structure function results for the 10 bit data collected after 2 June 1987. Table 11 presents the same results for the variance method. With the 10 bit data, instrument sensitivity is between 0.20 and 0.06 Kelvins/count (5.0 - 16.7 counts/Kelvin from Table 6) for typical scene temperatures. This allows for the digitization of the low amplitude noise in the scene data.

Case 4 presents noise estimates over a thermal scene on 4 June 1987. Ten bit data were collected in all three window channels for this flight. Although noise estimates are somewhat higher than expected, possibly from natural scene variability and error in extrapolation of the structure curves to zero separation distances, a definite reduction in noise is seen when comparing Case 4 to earlier 8 bit cases. This is especially evident in the variance method where noise estimates were reduced by a factor of two. Structure function along track estimates may also indicate some line-to-line calibration fluctuation (increasing structure in the along track direction) since these estimates exceed across track values.

In cases 5 and 6, more uniform thermal scenes were acquired which allowed for reliable noise estimates. The two cases differ only in the channel configuration. In each case, the isotropic 10 bit noise estimates are less than 0.28 Kelvins. A few values are less than the sensitivity of the 10 bit infrared channels (less than 0.10 Kelvins). This is encouraging since it indicates that relative scene variations of 0.10 to 0.30 Kelvins can be attributed to real scene fluctuations. This is a substantial improvement over previous 8 bit configurations. This high degree of precision is very valuable in quantitative calculations for scientific investigations. Variance method noise estimates generally support the structure function estimates, with the exception of the 3.7 micrometer data. However, reliable estimates of noise in the 3.7 micrometer channel are difficult to obtain due to the susceptibility of this channel to reflected solar contamination.

-----

Table 11

Single sample noise calculations based on scene variance for six different MAMS flights. The values were computed over the identical regions as in Table 10. Values can be compared to those of the "isotropic" values in Table 10. All units are in Kelvins. See text for further discussion.

Case 1: 22 Jan 85 (8 bit)

| Channel | Band | Scene Temp | w/o avg | 31 line avg |
|---------|------|------------|---------|-------------|
| 9       | 6.5  | 244        | .76     | .65         |
| 10      | 6.5  | 244        | .84     | .71         |
| 11      | 11.1 | 278        | .23     | .13         |
| 12      | 12.5 | 278        | 4.43    | 2.43        |

Case 2: 5 July 86 (8 bit)

| Channel | Band | Scene Temp | w/o avg | 31 line avg |
|---------|------|------------|---------|-------------|
| 9       | 6.5  | 236        | .59     | .53         |
| 10      | 11.1 | 287        | .45     | .36         |
| 11      | 11.1 | 287        | .30     | .30         |
| 12      | 12.5 | 282        | .65     | .66         |

Case 3: 29 May 87 (8 bit)

| Channel | Band | Scene Temp | w/o avg | 31 line avg |
|---------|------|------------|---------|-------------|
| 9       | 3.7  | 291        | .60     | .60         |
| 10      | 3.7  | 291        | .62     | .57         |
| 11      | 11.1 | 292        | .22     | .22         |
| 12      | 12.5 | 289        | .28     | .22         |

Case 4: 4 June 1987

| Channel | Band | Scene Temp | 10 bit data |
|---------|------|------------|-------------|
| 9       | 3.7  | 296        | .32         |
| 10      | 3.7  | 296        | .35         |
| 11      | 11.1 | 297        | <.05        |
| 12      | 12.5 | 292        | .17         |

Table 11 (continued)

Case 5: 7 June 87

| Channel | Band | Scene Temp | 10 bit data |
|---------|------|------------|-------------|
| 9       | 6.5  | 238        | .27         |
| 10      | 6.5  | 239        | .17         |
| 11      | 11.1 | 297        | <.05        |
| 12      | 12.5 | 292        | .20         |

Case 6: 27 Jan 88

| Channel | Band | Scene Temp | 10 bit data |
|---------|------|------------|-------------|
| 9       | 3.7  | 284        | .48         |
| 10      | 3.7  | 283        | .37         |
| 11      | 11.1 | 284        | <.05        |
| 12      | 12.5 | 282        | .13         |

---

#### D. Relative and Absolute Accuracy

The relative and absolute accuracy of the MAMS infrared data has been evaluated through comparisons with other absolutely calibrated remote sensing instruments. Observations from the High resolution Interferometer Sounder (HIS) (Smith et al., 1988), the Advanced Very High Resolution Radiometer (AVHRR) (Schwalb, 1982), and the VISSR Atmospheric Sounder (VAS) (Montgomery and Uccellini, 1985) have been collocated in space and time with the MAMS data for selected case studies. While no one instrument serves as an absolute calibration source, agreement between independent instruments tends to indicate that the MAMS is fairly well calibrated. All of the MAMS and other remote sensor data that were used for the following comparisons have been checked for bad data (bit errors, missing pixels, bad blackbody and calibration values) and corrected where possible. In all of the following comparisons, error in the HIS, AVHRR, and VAS data were not considered.

MAMS and HIS calibrations were compared with data from 15 June 1986. Both instruments flew onboard a NASA U2 aircraft over the COHMEX region on this day, thus enabling good collocation (in space and time). The HIS, a nadir viewing Michelson interferometer with a 2 km field of view, is calibrated by viewing a warm and a cold blackbody source every two minutes. As indicated in section III B, the MAMS does likewise every sixth of a second. The HIS spectral radiances (at roughly 0.5 wavenumber resolution) were convolved with the MAMS spectral response functions to produce a HIS radiance determination corresponding to each MAMS infrared channel. The comparison was then made between this HIS radiance data and the collocated MAMS data that have been averaged over the HIS footprint. Since the MAMS spectral response function is well known (to within 1 wavenumber resolution), the HIS high spectral resolution provides an excellent opportunity for comparison. The three channel comparison (6.5, 11.1, and 12.5 micrometers) for data along a portion of the flight track of 15 June 1986 is shown in Figs. 10 - 12 and the statistics for roughly 350 intercomparisons from the entire flight are presented in Table 12.

All three channels exhibit high correlations indicating that the MAMS and HIS instruments are observing similar relative variations in the scene. This agreement is readily apparent in the 6.5 micrometer data (Fig. 10), but it is more difficult to see in the 11.1 and 12.5 micrometer data (Figs. 11 and 12) because of the large scene variation for these surface viewing channels. The good agreement is more apparent when the aircraft flew over a cumulonimbus cloud (not shown), as both the MAMS and HIS brightness temperatures drop to colder values. Bias and RMS deviations (with respect to the bias) for the 6.5 micrometer data are found in Table 12 to be very good (-0.06 and 0.80 Kelvins, respectively). For the 11.1 and 12.5 micrometer

# MAMS/HIS 6.5 MICRON

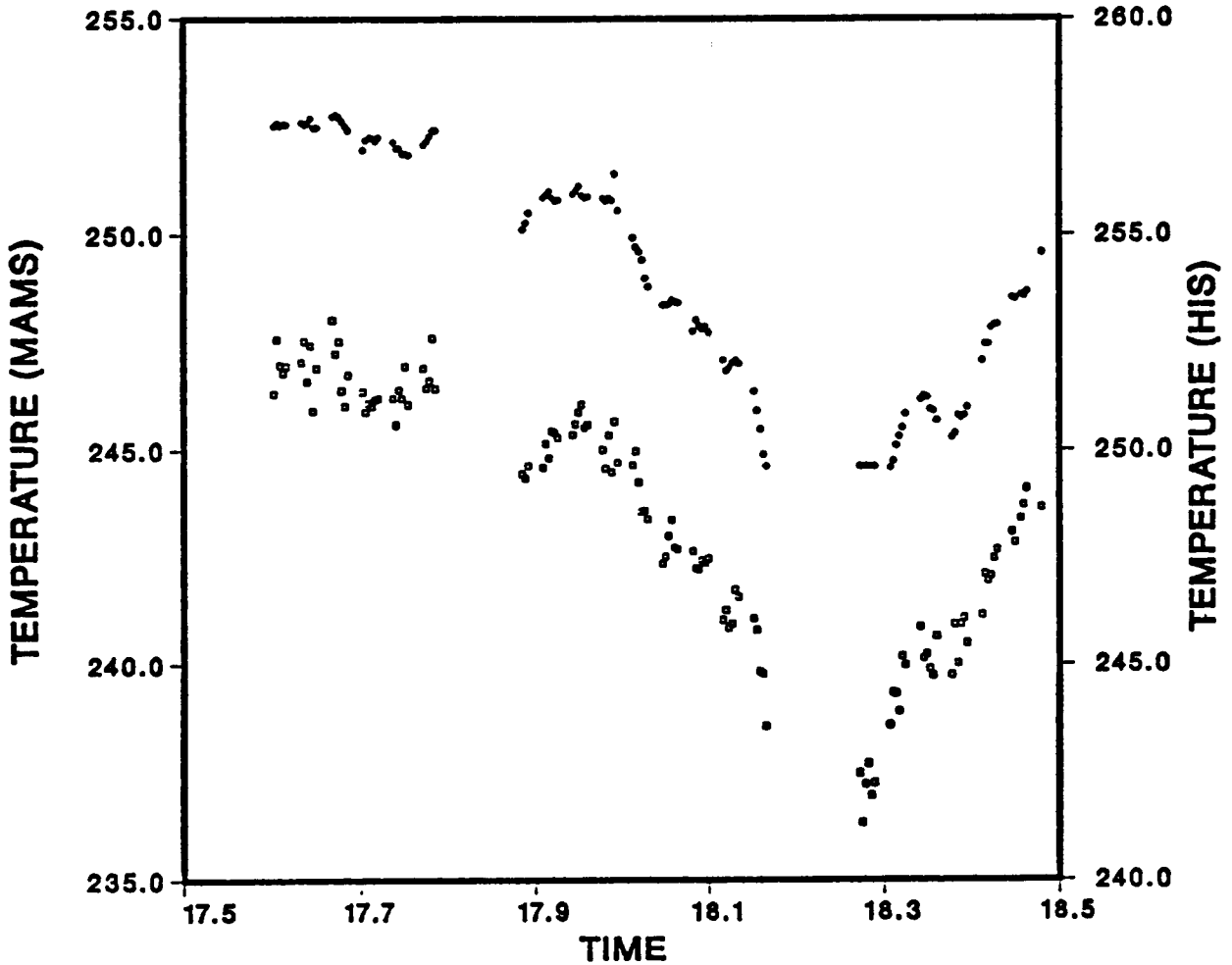


Figure 10. Comparison of MAMS (filled circles) and HIS (open squares) 6.5 micrometer channel data for a portion of the joint instrument flight of 15 June 1986. The vertical axis indicates the average scene temperature (Kelvins) derived from collocated fields of view. Note that the HIS temperature axis has been lowered by 5 degrees for clarity. See text for further discussion.

# MAMS/HIS 11.1 MICRON

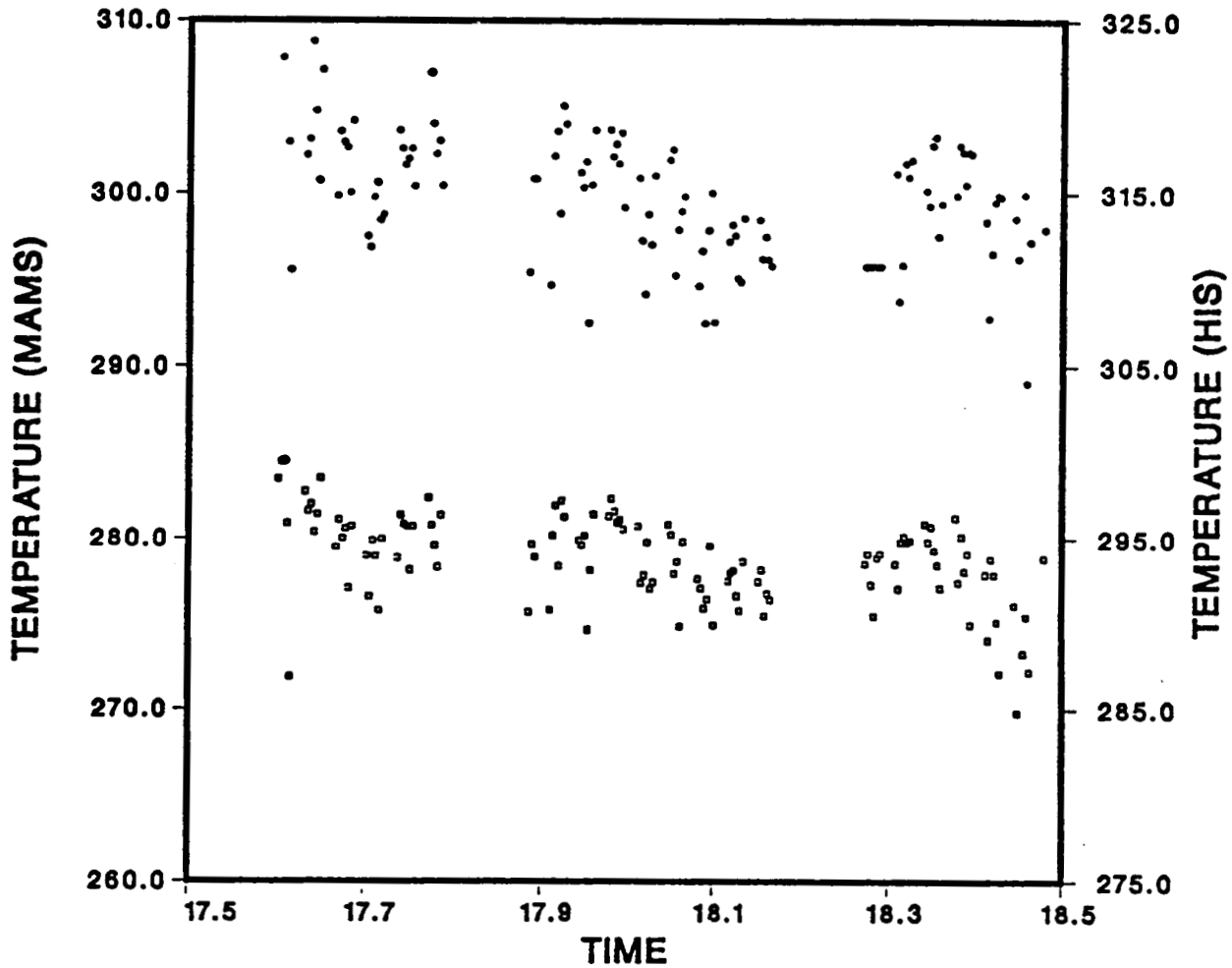


Figure 11. Comparison of MAMS (filled circles) and HIS (open squares) 11.1 micrometer channel data for a portion of the joint instrument flight of 15 June 1986. The vertical axis indicates the average scene temperature (Kelvins) derived from collocated fields of view. Note that the HIS temperature axis has been lowered by 15 degrees for clarity. See text for further discussion.

# MAMS/HIS 12.5 MICRON

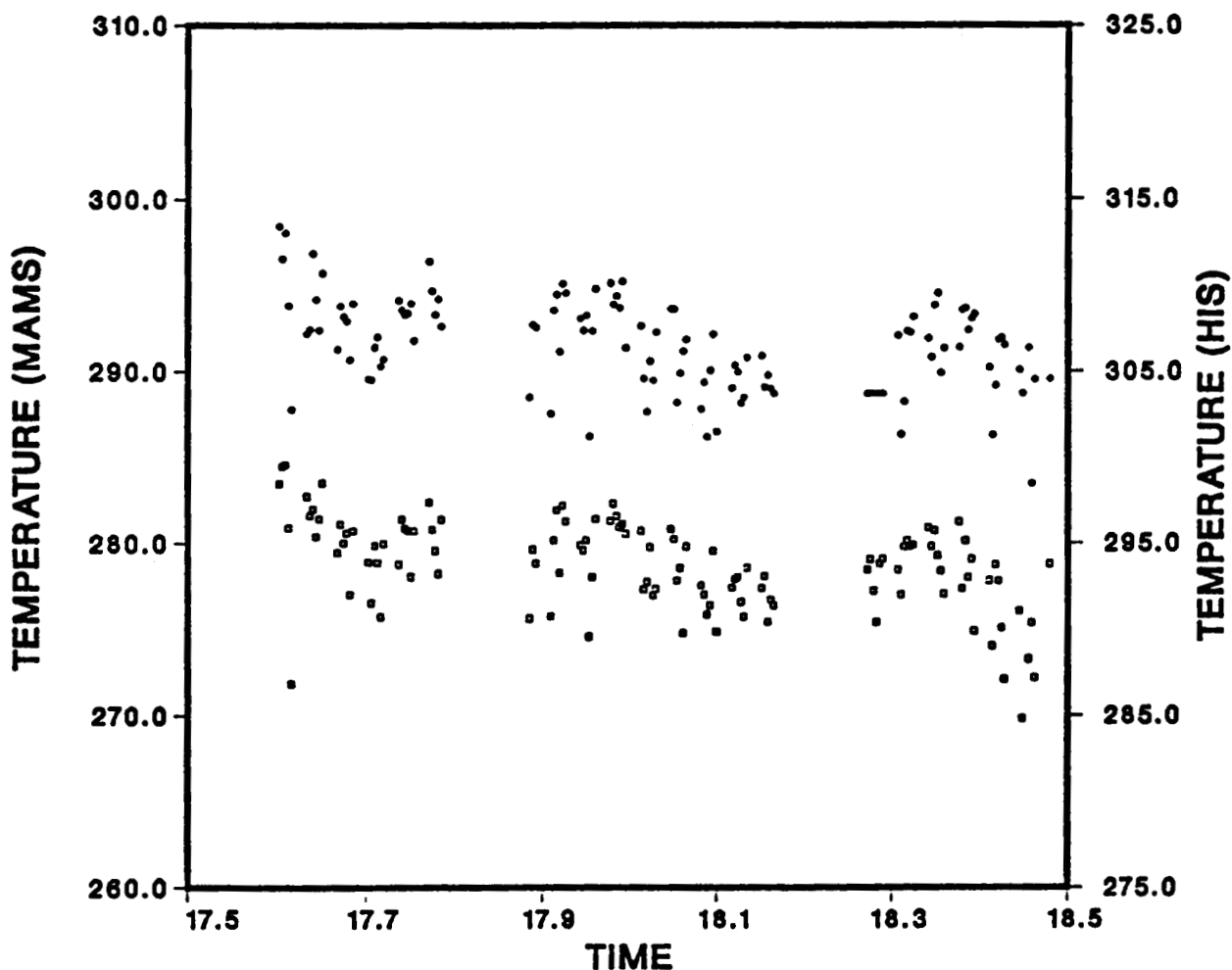


Figure 12. Comparison of MAMS (filled circles) and HIS (open squares) 12.5 micrometer channel data for a portion of the joint instrument flight of 15 June 1986. The vertical axis indicates the average scene temperature (Kelvins) derived from collocated fields of view. Note that the HIS temperature axis has been lowered by 15 degrees for clarity. See text for further discussion.

-----

Table 12

MAMS intercomparisons with HIS on 15 June 1986 for three of the four infrared channels. The upper set of numbers presents the results for 350 clear and partly cloudy fields of view. The lower set presents the results for 11 clear fields of view. See text for discussion.

350 Fields of View

| Channel | Bias (MAMS-HIS)<br>(Kelvins) | RMS Deviation<br>(Kelvins) | Correlation |
|---------|------------------------------|----------------------------|-------------|
| 6.5     | -0.06                        | 0.80                       | 0.98        |
| 11.1    | 0.85                         | 3.31                       | 0.94        |
| 12.5    | -2.43                        | 2.52                       | 0.95        |

11 Clear Fields of View

| Channel | Bias (MAMS-HIS)<br>(Kelvins) | RMS Deviation<br>(Kelvins) | Correlation |
|---------|------------------------------|----------------------------|-------------|
| 11.1    | 0.75                         | 0.36                       | 0.99        |
| 12.5    | -1.89                        | 0.48                       | 0.97        |

-----

comparisons, these statistics are somewhat less favorable due in part to a significant coverage of small cumulus clouds. Small errors in the navigation can cause spatial offsets between the two instruments and affect the portion of the field of view covered by cloud. In a field with small scattered cumulus clouds, these offsets could be the difference between looking at the earth's surface between clouds or looking at part of the cumulus cloud in the field of view. The same effect occurs when viewing a highly varying surface temperature field (which occurred in the 15 June data).

In an attempt to remove this field of view uncertainty in the comparisons, a small sample data set of clear fields of view over a relatively uniform surface temperature scene was used to generate the statistics presented in the lower half of Table 12. This second set of statistics shows a similar bias and a reduced deviation for both surface viewing channels (.75 and .36 Kelvins for 11.1 micrometers and -1.89 and .48 Kelvins for 12.5 micrometers). Thus by reducing the effects of small navigation

errors, the RMS deviations for both window channels are less than 0.5 Kelvins. Because only eleven comparisons provided the statistics, these results are not definitive but they do indicate close agreement between the two instruments in clear conditions.

The AVHRR instrument onboard the polar orbiting NOAA TIROS-N series of satellites was also compared to the MAMS using data from 27 January 1988. On this day, the MAMS was flown along the Louisiana coastline from 1430 GMT to about 1630 GMT, while the NOAA 10 satellite passed over the region at about 1430 GMT. The AVHRR data are calibrated every sixth of a second with a space and blackbody view and an assumption of linear detector response. This is comparable to the MAMS calibration with the exception that MAMS views two on-board blackbodies. For the comparisons, corrections for differing spectral response and view angles were made with forward radiance calculations using a known atmosphere. MAMS data were averaged over a given AVHRR field of view (approximately 1 km) to account for spatial resolution differences. Comparisons were made between the AVHRR channel 4 (10.5 micrometers) and the MAMS channel 11 (11.1 micrometers); NOAA 10 does not have a 12.5 or a 6.5 micrometer channel. Figures 13 and 14 show the infrared imagery from both systems for this day.

Comparisons were done primarily on collocated fields of view over water in the Gulf of Mexico, thus minimizing both the effects of time differences between the observations and the navigation errors. Table 13 shows the results of almost 100 intercomparisons. The MAMS and AVHRR demonstrate a sizable bias, but are roughly within one degree deviation of that bias. Figures 13 and 14 clearly show that the horizontal gradients of the MAMS are in excellent agreement with the AVHRR data. Much small scale variability is present in the MAMS data at scales below that of the AVHRR (1 km) data. Sensitivity to less than 0.10 Kelvin is apparent in both images.

-----  
 Table 13

MAMS Intercomparisons with AVHRR data on 27 January 1988 for the 11 micrometer channel. See text for discussion.

95 Fields of View

| Channel | Bias (MAMS-AVHRR)<br>(Kelvins) | RMS Deviation<br>(Kelvins) | Correlation |
|---------|--------------------------------|----------------------------|-------------|
| 11.1    | 4.44                           | 1.08                       | 0.91        |

-----

ORIGINAL PAGE IS  
OF POOR QUALITY

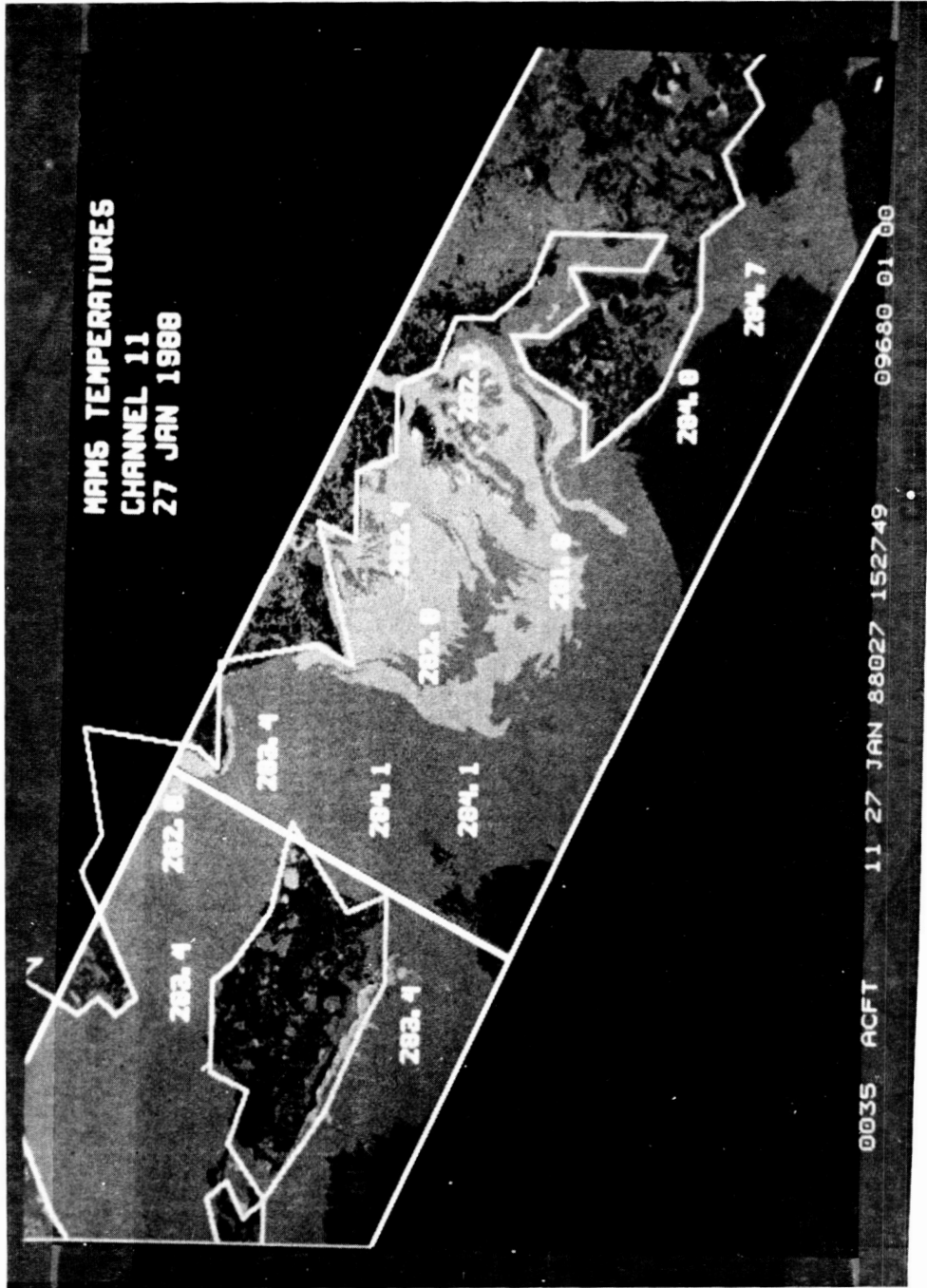


Figure 13. MAMS 11.1 micrometer data along the Louisiana coastline on 27 January 1988 at 1530 GMT. The data have been remapped into a common projection with that of Fig. 14 for comparison. The diagonal white line denotes missing data while the jagged line defines the land/water boundary.

ORIGINAL PAGE IS  
OF POOR QUALITY

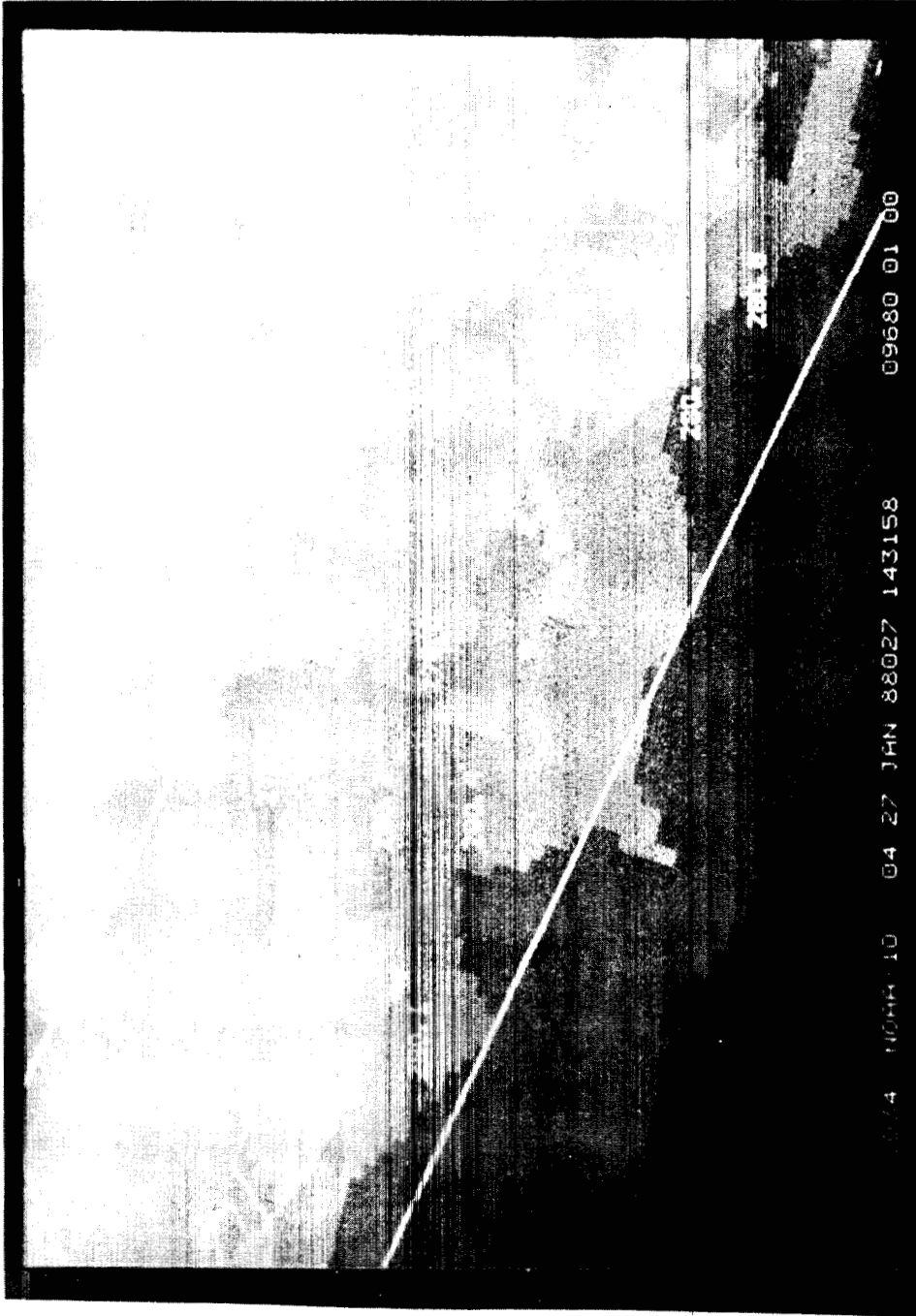


Figure 14. AVHRR 10.8 micrometer data along the Louisiana coastline on 27 January 1988 at 1430 GMT. The data have been remapped into a common projection with that of Fig. 13 for comparison. Note that the land is cooler than in the MAMS imagery (Fig. 13) because of the time difference (1 hour) between the MAMS and AVHRR data.

The VAS instrument on board the geostationary GOES satellite was compared with MAMS data on four separate days, each having a different MAMS configuration or weather situation. The VAS is calibrated every 1.6 seconds using space and blackbody references. Two MAMS flights over the COHMEX region (15 and 19 June 1986) were compared with nearly simultaneous observations from the VAS channels 7 (12.7 micrometer), 8 (11.2 micrometer), and 10 (6.7 micrometer). Two additional flights over water near the Atlantic coastline on 29 May 1987 and the Gulf of Mexico on 27 January 1988 were also compared; the latter is noteworthy because it is the first ten bit data available from the MAMS over an extensive water surface. The VAS comparisons were accomplished in a similar fashion to the AVHRR comparisons; collocated data are corrected for spectral differences as well as viewing geometry differences. MAMS data were averaged to match the VAS field of view (6.9 km for the 11.1 and 12.7 micrometer channels and 13.8 km for the 6.7 micrometer channel); when possible corrections for navigation errors were made.

Table 14 shows the results of the MAMS and VAS comparisons, which number between 25 to 75 for each day. It is apparent that the bias varies from day to day as the MAMS instrument configuration is altered (gain and offset in the thermal channels were adjusted in between these flights), but the deviation with respect to the bias remains somewhat unchanged. The biases for flights after COHMEX are generally smaller; this is at least partially the result of the instrument improvements cited in section IIB. Some of the lower correlation coefficients can be attributed to a small spread in the observed brightness temperatures in the intercomparison; the good deviation values bear this out. Exact collocation of the large VAS ifovs with the high resolution MAMS data may account for some of the variability.

In summary, the MAMS radiometer has been compared with three other infrared sensing instruments. Determination of the quality of the absolute calibration remains elusive; this is very sensitive to good collocation of the fields of view. The MAMS-HIS comparisons eliminated most of the time/ space/ sensor platform/ spectral channel differences and probably represent the most accurate estimate of absolute calibration. The bias of MAMS with respect to other observations seems to be sensitive to the MAMS instrument configuration and should be tracked on a day to day basis. The relative calibration of MAMS with respect to the other observations is very good; the deviation with respect to the bias is usually less than two Kelvins. The horizontal gradients measured by the MAMS correspond very well with those of other coarser resolution instruments.

Table 14

MAMS Intercomparisons with VAS data on selected dates and for different instrument configurations. See text for discussion.

| Channel | FOVs | Date    | Bias<br>(MAMS-VAS)<br>(Kelvins) | RMS<br>Deviation<br>(Kelvins) | Correlation |
|---------|------|---------|---------------------------------|-------------------------------|-------------|
| 6.5     | 75   | 6/15/86 | -3.51                           | 1.00                          | .94         |
|         | 69   | 6/19/86 | -2.78                           | 1.10                          | .73         |
| 11.1    | 75   | 6/15/86 | 2.76                            | 2.05                          | .61         |
|         | 69   | 6/19/86 | 4.94                            | 1.81                          | .66         |
|         | 25   | 5/29/87 | 0.44                            | 1.61                          | .81         |
|         | 74   | 1/27/88 | 1.80                            | 1.86                          | .52         |
| 12.5    | 75   | 6/15/86 | -1.36                           | 1.90                          | .62         |
|         | 69   | 6/19/86 | 1.01                            | 1.71                          | .55         |
|         | 25   | 5/29/86 | -0.11                           | 1.87                          | .33         |
|         | 74   | 1/27/88 | 2.33                            | 1.78                          | .43         |

## IV. NAVIGATION OF DATA

### A. Data Sources

In order to navigate MAMS data accurately, both the subpoint position of the aircraft and the scanner position must be known. The information necessary to determine these values is routinely recorded on cassette tape during aircraft data collection flights through an Inertial Navigation System (INS) onboard the aircraft. The important quantities recorded are time, subpoint latitude and longitude, and aircraft heading and altitude. This INS data are recorded approximately every five seconds.

The MAMS multispectral data are collected concurrently with header information (calibration, time, etc.) and are recorded for each scan of the instrument onto 14 track tape. The MAMS scene data are navigated by combining these two data sources through their common recording of time.

### B. Navigation Relationships for MAMS

A methodology which navigates MAMS data for one straight line segment of a flight track was chosen because it allows the INS data to be represented by a simple set of linear regression coefficients. This reduces the rather large INS data file down to several sets of linear regression coefficients. In the following discussion a straight line flight track is defined to be one in which latitude and longitude changes are a linear function of time.

In developing navigation relationships for a straight line flight track, coefficients are produced from the INS data for subpoint latitude and longitude, and aircraft heading and altitude versus time. The INS data have been filtered for bad data and are corrected wherever possible. The generated regression coefficients are stored in a file, along with other housekeeping information. The aircraft subpoint is determined by first finding the time of each MAMS scan line

$$t = t_0 + (S - S_0) / r \quad (11)$$

where

- $t_0$  is the time of first line of recorded data of straight line flight track,
- $S$  is the recorded line number of each data line,
- $S_0$  is the recorded line number of first data line, and
- $r$  is the instrument scanning rate (constant).

This time quantity is applied in the regression relationships for subpoint latitude and longitude,

$$\text{LAT}_s = a * t + b \quad (12)$$

$$\text{LON}_s = c * t + d \quad (13)$$

where a,b,c, and d are the regression coefficients computed earlier. The scanner angle (DD) is obtained from the data element location in the scan line and the scanner characteristics

$$\text{DD} = K * (E - E_n) \quad (14)$$

where

DD is the displacement (in degrees) from subpoint,  
 K is the angular distance between ifovs (85.92 degrees/ 715 steps between ifovs, which is constant),  
 $E_n$  is the nadir element (358.5), and  
 E is the individual element number in the data line.

The distance D from the aircraft subpoint to the data element is then given by

$$D = Z * \tan(\text{DD}) \quad (15)$$

where Z is the aircraft altitude expressed as

$$Z = e * t + f \quad (16)$$

In (16) the altitude is assumed to be that of the altitude above ground level.

In order to determine latitude and longitude coordinates on the earth, the spherical triangle shown in bold outline in Fig. 15 is used. The known quantities in this triangle are the subpoint latitude, the distance D along the scan line, and the included surface angle (aircraft heading  $-90^\circ$ ) where the heading (H) is given by

$$H = g * t + h \quad (17)$$

This triangle is solved using the laws of cosines and sines to determine the latitude and longitude values of the image coordinates.

An inverse navigation transform is used to determine MAMS image coordinates from latitude and longitude coordinates. This procedure allows for cartographic overlays and remapping of MAMS data into more universal projections.

The algorithm is initialized with the given Earth location, the aircraft location at the beginning of the flight track, and the direction of the flight track (from the latitude/ longitude regression fits). These three quantities, along with the scan



line through the Earth location perpendicular to the flight track, define the dimensions and location of a right triangle in the scan image (Fig. 16). In this triangle, the distance traveled along the flight track and hence the elapsed time are obtained. The aircraft heading at this time is used to rotate the scan line so that it is perpendicular to the heading. The aircraft nadir point and elapsed time are adjusted correspondingly. The instrument scan rate, with the elapsed time, is used to compute the number of scan lines to the given Earth location in the image. The distance along the scan line from nadir to the input Earth location is used to compute the element number.

### C. Error Sources and Bias Correction

One of the drawbacks of using a linear regression scheme to represent the INS data is that deviations in the measured parameters will cause scatter in the regression and thus error in the navigation. Table 15 lists the RMS values for straight line flight tracks during the COHMEX case studies. The RMS values of latitude and longitude for all flight tracks are within about 0.5 km error, although variations in the RMS are apparent from flight track to flight track. RMS error values for heading and altitude represent error incurred at maximum scan angle ( $43^{\circ}$ ). These errors go to zero at aircraft nadir. Variation in RMS may be due to several factors, such as autopilot over-adjustment, and changes in aircraft heading with respect to prevailing winds. The navigation will incur the least error at aircraft subpoint and the most at the limit of the instrument scan angle (i.e., 43 degrees) where aircraft heading and altitude error have their greatest impact on the geometry. In addition to linear regression error, there is also small (<100m) error due to approximations to earth geometry.

Additional error sources may exist if there are biases between the INS data and the earth or between the INS time recording and the MAMS scan line time recording. Errors of this nature can be large, but in many cases are correctable through the use of a separate bias correction for latitude, longitude, and time. Such a correction is made by comparing known locations (e.g., rivers and crossroads) in the MAMS imagery to the navigation specified location. If several locations are compared in this manner, a simple bias can be computed.

Although the navigation errors do exhibit some fluctuation (and bias corrections are not always possible), the MAMS imagery can in general be navigated to an accuracy of about 0.5 km. For the earth location of atmospheric features and coarse resolution satellite intercomparisons, such accuracy is very acceptable. With the use of landmarks (when available) and careful determination of bias corrections, individual flight tracks have been navigated down to the resolution of individual ifovs (100m).

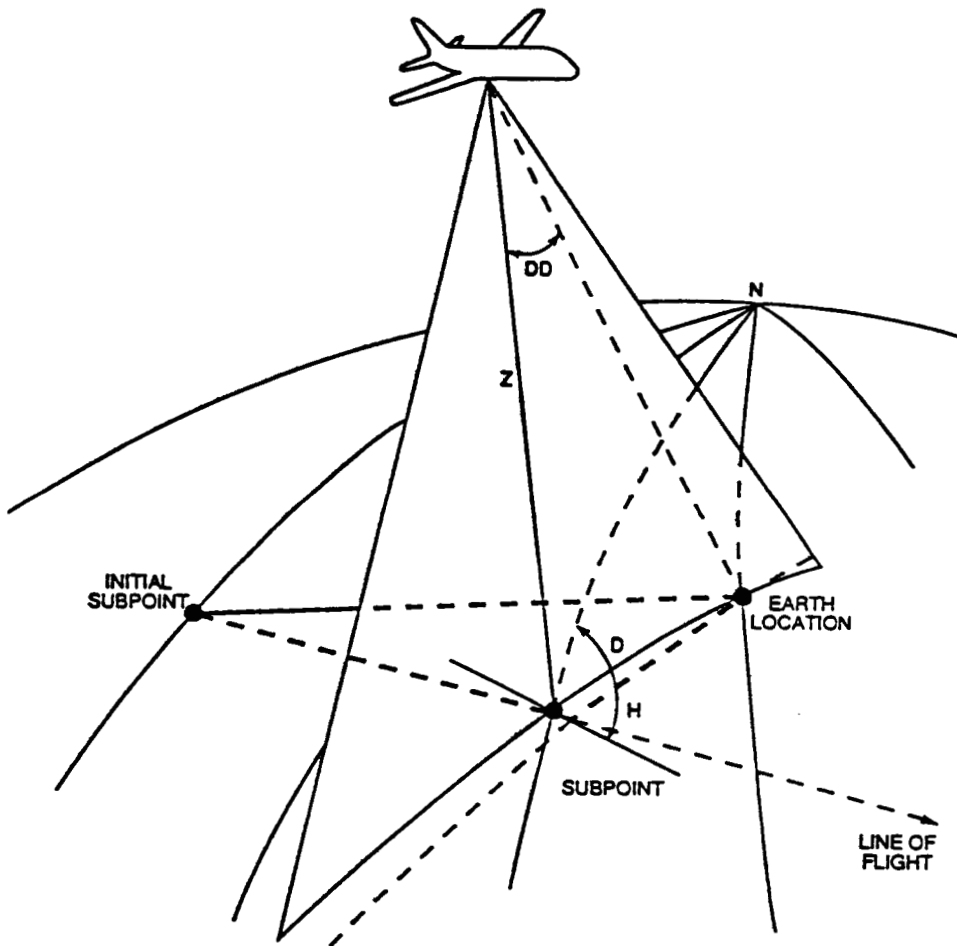


Figure 16. Schematic diagram indicating the geometry used in the navigation of MAMS imagery in order to locate a given earth coordinate in the image data (inverse transform). See text for discussion.

Table 15

MAMS Navigation RMS Data

| Date<br>Flight Track | Latitude<br>(km) | Longitude<br>(km) | Heading<br>(km) | Altitude<br>(km) |
|----------------------|------------------|-------------------|-----------------|------------------|
| June 15, 1986        |                  |                   |                 |                  |
| A - B                | .199             | .297              | .222            | .026             |
| C - D                | .414             | .532              | .278            | .019             |
| E - F                | .361             | .347              | .223            | .050             |
| G - H                | .207             | .322              | .110            | .039             |
| I - J                | .207             | .262              | .168            | .035             |
| June 18, 1986        |                  |                   |                 |                  |
| B - C                | .248             | .208              | .182            | .023             |
| D - E                | .470             | .222              | .217            | .019             |
| F - G                | .156             | .174              | .248            | .030             |
| H - I                | .330             | .427              | .295            | .029             |
| J - K                | .293             | .221              | .251            | .037             |
| L - M                | .414             | .361              | .348            | .042             |
| N - O                | .258             | .382              | .278            | .024             |
| June 19, 1986        |                  |                   |                 |                  |
| B - C                | .379             | .167              | .215            | .025             |
| D - E                | .233             | .175              | .214            | .026             |
| F - G                | .374             | .272              | .244            | .062             |
| H - I                | .466             | .180              | .246            | .025             |
| F - G(2)             | .383             | .490              | .251            | .063             |
| H - I(2)             | .324             | .292              | .171            | .012             |
| June 26, 1986        |                  |                   |                 |                  |
| B - C                | .223             | .700              | .183            | -                |
| C - D                | .219             | .400              | .240            | -                |
| D - E                | .407             | .496              | .130            | -                |
| E - F                | .332             | .277              | .219            | -                |
| F - G                | .488             | .318              | .162            | -                |
| G - H                | .257             | .428              | .256            | -                |

## V. FLIGHT INFORMATION

### A. Recent Flights

A number of engineering and science flights have taken place since the last report. These flights have been in different geographic regions, in different seasons, at different times of the day, and under a variety of weather/ cloud cover conditions. Thus, the data can be useful for many science applications. Tables C1 - C3 of Appendix C present flight details for 1986 through 1988 activities, which includes the COHMEX case studies. The instrument configurations for these flights were discussed previously (Table 1) . Appendix D presents the flight tracks for most of these flights based on the aircraft INS data.

MAMS flight activity is usually coordinated around major field experiments to support ground-based and satellite measurements. The science flights of 1985 (listed in the previous report) and those of 1986 were conducted in-conjunction with measurements of the pre-convective environment. The 1986 flights were coordinated with the COHMEX project during which an extensive ground observation network was operating (Arnold, 1986). The MAMS was flown in conjunction with other infrared and microwave radiometers at this time. The MAMS was also used to collect data over the Konza Prairie region of Kansas during FIFE (Sellers and Hall, 1987).

### B. Data Availability

Many flights have been made with MAMS since 1985. The data collected are of good quality and have captured many interesting features. General quality of the data for each series of flights has been discussed in section IIIC. Data from the 1987 and 1988 flights probably are comparable to that from the AVHRR instrument on the NOAA polar orbiting flights in terms of noise and radiometric accuracy. Any data collected with MAMS can be obtained from NASA for scientific investigations. Details on how to obtain this data are presented in the Appendix E.

## VI. SCIENCE APPLICATIONS

The remotely sensed MAMS data have been applied to a number of different research topics. Some of them are highlighted below.

### A. Low-level Precipitable Water Determination

A new technique has been developed which uses MAMS split window channel radiance fields to derive quantitative estimates of mesoscale precipitable water variability. The Split Window Variance Ratio (SWVR) technique relates image radiance variance to atmospheric transmittance. The transmittance ratio is correlated with the low-level precipitable water values. A complete description of the technique and case study evaluations are available in Jedlovec (1987) and Jedlovec (1988).

The derived low-level precipitable water product can be combined with the mid-tropospheric water vapor channel (6.5 micrometer) to provide two layers of mesoscale moisture variability for diagnostic analysis. This imagery is also being studied for its use in deriving a mesoscale stability map (a combination of surface skin temperature, low-level precipitable water, and mid-tropospheric temperature and moisture).

Work is proceeding to evaluate the SWVR technique using AVHRR data. The AVHRR split window channels, although less sensitive to low-level precipitable water, provide very accurate, medium resolution data to monitor water vapor variations. Successful application will yield enhanced capabilities for the operational community. Application of the SWVR technique to VAS data is not expected to be useful because the technique requires high spatial resolution data over which scene variances are calculated.

### B. Relationship Between Surface Features, Clouds, and Precipitable Water

Visible satellite measurements of cumulus cloud development indicate preferential regions for growth, particularly in association with orography. COHMEX data are being investigated to evaluate the role of surface topography, land scene class, and low-level moisture play in determining cloud cover under particular atmospheric flow regimes. The 19 June data sets from MAMS, AVHRR, and GOES are being used to map low-level water vapor patterns, surface skin temperature, and surface class type (water, forest, bare soil, urban, etc.) in order to evaluate interactions of the surface features with the lower portion of the atmosphere.

A mesoscale numerical model is also used to evaluate the

predictability of these cloud features and their spatial locations and distribution. Preliminary work indicates that the lower boundary temperature and scene type may be extremely important in cloud distribution. Efforts will begin to incorporate MAMS derived skin temperature and low-level precipitable water into the mesoscale model to further study this effect.

#### C. MAMS/VAS Combined Precipitable Water and Stability

Extensive efforts have been made to combine MAMS and VAS data in order to produce a high resolution image/sounding product. The high temporal resolution available with VAS makes it a desirable sensor to monitor environmental changes in the relatively cloud-free environment. Higher spatial resolution data are available at wavelengths sensitive to atmospheric water vapor several times a day (AVHRR) or for limited case studies (MAMS). The motivation for this work stems from a need to diagnose mesoscale moisture and stability at smaller scales than currently available (VAS capabilities seem limited to scales of about 100 km). Demonstration of the ability to combine radiance measurements of this type to derive high resolution products supports future sensor development work.

Combining the VAS and MAMS data for product generation is more difficult than expected. When observed data from each sensor are compared for the same ifov (one VAS 8 km foot print) large biases are observed (see Section III). Presumably these biases occur because of four major instrument differences (spectral, spatial, calibration, and viewing geometry) and must all be considered in any data combination. The spectral channel differences are fairly easy to determine. Spatial resolution is accounted for by collocating data and averaging MAMS pixels over the VAS footprint. This is precise down to the navigation accuracy of the data (0.2 km for MAMS, 2.0 km for VAS at best). Absolute calibration of each data type has always been problematic but consistent inter-sensor bias can be handled appropriately. Because the atmospheric profiles are not well known, correction for viewing geometry is hindered. Despite these difficulties, systematic biases have been identified and corrections have been applied to combine the data. Results of 100m MAMS/VAS "retrievals" are encouraging and further applications and investigations are proceeding.

#### D. MAMS/HIS Combined Products for Diagnostic Investigations

High-resolution Interferometer Sounder (HIS) and MAMS data were simultaneously collected from many of the aircraft flights during COHMEX. The nadir viewing HIS provides very high spectral information from a 2 km region along the flight track line. High spatial resolution MAMS data are available at the same time. A combined display of MAMS imagery over the HIS 2 km footprint and

the HIS radiance spectrum over the MAMS spectral channel bandpass offers some very interesting new information. For example, changes in the level of moisture detected with MAMS at 6.5 micrometers can be readily observed by examining the changing absorption/ emission spectrum recorded by the HIS data. Similar changes can be seen in the low-level water vapor channels.

The common observation time and observation platform produces less problems in combining MAMS/HIS data than for VAS/MAMS data. Work is beginning on a combined HIS/MAMS sounding/imaging product similar to that described for VAS/MAMS above.

#### E. Surface Skin Temperature and Emissivity Mapping

MAMS data collected over Kansas in June 1987 are proving very useful for the analysis of MAMS capabilities for land processes. Three window channels (3.7, 11.1, and 12.5 micrometers) were used to collect upwelling radiance measurements over a limited region "ground truthed" with in-situ and low altitude aircraft sensors. This data collected from MAMS are of excellent quality. With the appropriate channel sensitivities and 10 bit digitization, real variations of 0.1 Kelvin are discernible in the 11 micrometer channel. This unique data are being used to develop an algorithm to derive land surface "skin temperature" which accounts for varying emissivity in the 11 micrometer region (mainly due to the changes in mineral content of bare soil and between land class types). This technique will utilize an image scene classification (from MAMS visible channels) to correlate image scene type with infrared emissivity. An emissivity correction for the thermal channels then can be applied based on scene type alone. A day/night data set collected during this series of flights will also allow a detailed study of thermal fluxes in relation to vegetation cover.

#### F. Four-dimensional Water Vapor Structures

This work attempts to understand the four dimensional distribution of atmospheric water vapor through a comparison of ground based Lidar and MAMS aircraft measurements from a series of night flights in June of 1987 and day flights of June/ July 1988. Comparisons of low- and mid-tropospheric moisture variability diagnosed by each sensor will be evaluated. This effort and those described with HIS/MAMS comparisons will show the utility of using profile measurements of moisture (from other than a rawinsonde) to interpret water vapor imagery. Small amounts of mid-tropospheric moisture measured from rawinsondes are particularly suspect because of the long instrument response time at cold temperatures.

## G. Sea-surface Temperature Estimation and Sediment Mapping for Geomorphic Changes

MAMS split window channel imagery is being used to estimate sea surface temperatures in an analogous manner to operational techniques with AVHRR and GOES/VAS data. MAMS high spatial resolution values are being compared to the SST derived from the other instruments as part of an under-flight program to inter-compare the measurements and derived products. Variations in sea surface temperatures are associated with ocean currents and upwelling patterns. These features occur at scales much finer than originally diagnosed. Additionally, the surface water temperatures may be related to water depth and sea state. When combined with sediment content mapped by visible channel imagery, the MAMS may provide a way to diagnose geomorphic changes in shallow bays and delta regions. This is a major objective of the geomorphic mapping flights of January 1988 and those planned for March of 1989.

## Appendix A: List of Acronyms

|         |  |
|---------|--|
| ADC     | Analog to Digital Converter  |
| AOCI    | Airborne Ocean Color Imager  |
| AVHRR   | Advanced Very High Resolution Radiometer                             |
| COHMEX  | CO-operative Huntsville Meteorological EXperiment                    |
| DC      | Direct Current   |
| Eos     | Earth Observation System   |
| ESS     | Earth System Science   |
| FIFE    | First ISLSCP Field Experiment  |
| fov     | field of view  |
| GOES    | Geostationary Orbiting Environmental Satellite                       |
| GMT     | Greenwich Mean Time  |
| HIS     | High-resolution Interferometer Sounder                               |
| ifov    | instantaneous field of view  |
| INS     | Inertial Navigation System   |
| IR      | Infrared   |
| MAMS    | Multispectral Atmospheric Mapping Sensor                             |
| McIDAS  | Man-computer Interactive Data Access System                          |
| MSFC    | Marshall Space Flight Center   |
| MODIS-N | MODerate-resolution Imaging Spectrometer                             |
| NASA    | National Aeronautics and Space Administration                        |
| NOAA    | National Oceanic and Atmospheric Administration                      |
| RMS     | Root Mean Square   |
| SST     | Sea Surface Temperature  |
| SWVR    | Split Window Variance Ratio  |
| TMS     | Thematic Mapper Simulator  |
| VAS     | Visible Infrared Spin Scan Radiometer (VISSR)<br>Atmospheric Sounder |

## Appendix B: Visible Channel Calibration Values

Section III.A. described the procedures used to convert raw count values to radiances received by the instrument in the visible channels. This conversion is linear and depends on the gain in each channel. The tables below list the calibration values (A) for most MAMS flights. Values for 1985, 1986, 1987, and 1988 are presented in Tables B1 - B4, respectively. YYDDD represents the year (YY) and julian day (DDD) of the flight. The letter M indicates that calibration data are not available. Conversion units are in  $\text{mW}/(\text{cm}^2\text{-um-ster})$ . See text for further discussion.

Table B1

| YYDDD |   | ch1  | ch2  | ch3  | ch4  | ch5  | ch6  | ch7  | ch8  |
|-------|---|------|------|------|------|------|------|------|------|
| 85021 | A | .273 | .170 | .140 | .425 | .280 | .260 | .196 | .115 |
| 85022 | A | .273 | .085 | .070 | .105 | .070 | .065 | .049 | .029 |
| 85024 | A | .074 | .082 | .074 | .124 | .248 | .089 | .094 | .062 |
| 85128 | A | .272 | .340 | .140 | .210 | .140 | .130 | .098 | .115 |
| 85129 | A | .272 | .340 | .140 | .210 | .140 | .130 | .098 | .115 |
| 85132 | A | .272 | .340 | .140 | .210 | .140 | .130 | .098 | .115 |
| 85136 | A | .272 | .340 | .140 | .210 | .140 | .130 | .098 | .115 |
| 85137 | A | .272 | .340 | .140 | .210 | .140 | .130 | .098 | .115 |
| 85138 | A | .272 | .340 | .140 | .210 | .140 | .130 | .098 | .115 |
| 85139 | A | .272 | .340 | .140 | .210 | .140 | .130 | .098 | .115 |
| 85140 | A | .272 | .340 | .140 | .210 | .140 | .130 | .098 | .115 |
| 85141 | A | .272 | .340 | .140 | .210 | .140 | .130 | .098 | .115 |
| 85143 | A | .272 | .340 | .140 | .210 | .140 | .130 | .098 | .115 |
| 85144 | A | .272 | .340 | .140 | .210 | .140 | .130 | .098 | .115 |
| 85173 | A | .254 | .230 | .350 | .400 | .280 | .280 | .150 | .084 |
| 85174 | A | .254 | .230 | .350 | .400 | .280 | .280 | .150 | .084 |
| 85175 | A | .254 | .230 | .350 | .400 | .280 | .280 | .150 | .084 |
| 85177 | A | .254 | .230 | .350 | .400 | .280 | .280 | .150 | .084 |
| 85233 | A | M    | M    | M    | M    | M    | M    | M    | M    |

B2

| YYDDD |   | ch1  | ch2  | ch3  | ch4  | ch5  | ch6  | ch7  | ch8  |
|-------|---|------|------|------|------|------|------|------|------|
| 86009 | A | M    | M    | M    | M    | M    | M    | M    | M    |
| 86010 | A | M    | M    | M    | M    | M    | M    | M    | M    |
| 86014 | A | M    | M    | M    | M    | M    | M    | M    | M    |
| 86016 | A | M    | M    | M    | M    | M    | M    | M    | M    |
| 86083 | A | .196 | .126 | .082 | .196 | .192 | .136 | .094 | .102 |
| 86085 | A | .196 | .126 | .094 | .196 | .192 | .136 | .094 | .102 |
| 86087 | A | .196 | .126 | .094 | .196 | .192 | .136 | .094 | .102 |

|       |   |      |      |      |      |      |      |      |      |
|-------|---|------|------|------|------|------|------|------|------|
| 86105 | A | M    | M    | M    | M    | M    | M    | M    | M    |
| 86106 | A | M    | M    | M    | M    | M    | M    | M    | M    |
| 86163 | A | .177 | .148 | .138 | .224 | .222 | .156 | .021 | .076 |
| 86164 | A | .177 | .148 | .138 | .224 | .222 | .156 | .021 | .076 |
| 86166 | A | .177 | .148 | .138 | .224 | .222 | .156 | .021 | .076 |
| 86169 | A | .177 | .148 | .138 | .224 | .222 | .156 | .041 | .076 |
| 86170 | A | .177 | .148 | .138 | .224 | .222 | .156 | .041 | .076 |
| 86177 | A | .177 | .148 | .138 | .224 | .222 | .156 | .041 | .076 |
| 86184 | A | .177 | .148 | .138 | .224 | .222 | .156 | .041 | .076 |
| 86186 | A | .177 | .148 | .138 | .224 | .222 | .156 | .041 | .076 |
| 86189 | A | .177 | .148 | .138 | .224 | .222 | .156 | .041 | .076 |
| 86192 | A | .177 | .148 | .138 | .224 | .222 | .156 | .041 | .076 |
| 86193 | A | .177 | .148 | .138 | .224 | .222 | .156 | .041 | .076 |
| 86201 | A | .177 | .148 | .138 | .224 | .222 | .156 | .041 | .076 |
| 86202 | A | .177 | .148 | .138 | .224 | .222 | .156 | .041 | .076 |

B3

| YYDDD |   | ch1   | ch2  | ch3  | ch4  | ch5  | ch6  | ch7  | ch8  |
|-------|---|-------|------|------|------|------|------|------|------|
| 87130 | A | .708  | .592 | .552 | .896 | .888 | .624 | .164 | .302 |
| 87149 | A | .708  | .592 | .552 | .896 | .888 | .624 | .164 | .302 |
| 87153 | A | .177  | .148 | .138 | .224 | .222 | .156 | .041 | .076 |
| 87155 | A | 1.000 | .054 | .100 | .123 | .069 | .100 | .071 | .270 |
| 87156 | A | 1.000 | .592 | .552 | .896 | .888 | .624 | .164 | .302 |
| 87157 | A | 1.000 | .148 | .138 | .224 | .222 | .156 | .041 | .076 |
| 87158 | A | 1.000 | .148 | .138 | .224 | .222 | .156 | .041 | .076 |

B4

| YYDDD |   | ch1   | ch2  | ch3  | ch4  | ch5  | ch6  | ch7  | ch8  |
|-------|---|-------|------|------|------|------|------|------|------|
| 88010 | A | M     | M    | M    | M    | M    | M    | M    | M    |
| 88027 | A | 1.000 | .022 | .022 | .228 | .031 | .023 | .034 | .006 |
| 88157 | A | 1.000 | .067 | .143 | .180 | .067 | .073 | .183 | .174 |
| 88162 | A | 1.000 | .067 | .143 | .180 | .067 | .073 | .183 | .174 |
| 88179 | A | 1.000 | .067 | .143 | .180 | .067 | .073 | .183 | .174 |
| 88180 | A | 1.000 | .067 | .143 | .180 | .067 | .073 | .183 | .174 |
| 88182 | A | 1.000 | .067 | .143 | .180 | .067 | .073 | .183 | .174 |
| 88190 | A | 1.000 | .067 | .143 | .180 | .067 | .073 | .183 | .174 |
| 88231 | A | 1.000 | .067 | .143 | .180 | .067 | .073 | .183 | .174 |
| 88238 | A | 1.000 | .067 | .143 | .180 | .067 | .073 | .183 | .174 |
| 88239 | A | 1.000 | .034 | .036 | .045 | .017 | .009 | .183 | .011 |

## Appendix C: MAMS Flight Information

The Tables below list general information about the MAMS flights which have taken place since the previous report. They provide information on the dates and locations of each flight. The numbers in parentheses after the date indicate the particular instrument configuration used for that flight. The asterisk (\*) before the location indicates that a flight track map is presented in Appendix D for this flight.

Table C1

MAMS flight information for February through December of 1986.

| Date     | Times<br>(GMT) | Location  | Comments            |
|----------|----------------|-----------|---------------------|
| 3-19 (1) |                | CA        | Engineering         |
| 3-24 (1) | 1933-2338      | CA/NV     | Cloud Studies       |
| 3-26 (1) | 1929-2335      | CA/NV     | Cloud Studies       |
| 3-28 (1) | 1833-2231      | CA/NV     | Cloud Studies       |
| 4-14 (1) |                | Kitt Peak | Data bad            |
| 4-15 (1) |                | Kitt Peak | Good data, with HIS |
| 4-16 (1) |                | Kitt Peak | Good data, with HIS |

### COHMEX Flights

|          |           |         |                                |
|----------|-----------|---------|--------------------------------|
| 6-12 (1) |           | CA      | ER2, MAMS test rh super pod    |
| 6-13 (1) |           | U.S.    | ER2, Ferry to Wallops, rh pod  |
| 6-15 (1) | 1600-2200 | *AL/TN  | U2, Sdg flight, 50% clds       |
| 6-18 (1) | 1330-2000 | *AL/TN  | U2, Sdg flight, clear          |
| 6-19 (1) | 1417-1913 | *AL/TN  | U2, Sdg flight, ER2 leads      |
| 6-26 (1) | 1628-2125 | *AL/TN  | U2, Rept coverage, BHM t-strm  |
| 7- 3 (1) | 1445-2030 | AL/TN   | U2, Sdg Flight, clear          |
| 7- 5 (1) | 1305-1730 | *Ocean  | U2, Buoy flight, w/HIS         |
| 7- 8 (1) | 1835-2350 | *AL/TN  | ER2, no roll correct, t-storms |
| 7-11 (1) | 1830-0100 | *AL/TN  | ER2, no roll correct, t-storms |
| 7-12 (1) | 1700-2300 | *AL/TN  | ER2, no roll correct, t-storms |
| 7-20 (1) | 1800-0015 | *AL/TN  | ER2, good data, t-storms       |
| 7-21 (1) | 1700-2315 | *E. Cst | ER2, good, t-storms over S. C. |

- (1). 6.5/11.1/11.1/12.5 micrometer channels used for the infrared bands 9 - 12.
- (2). 6.5/6.5/11.1/12.5 micrometer channels used for infrared bands 9 - 12.
- (3). 3.7/3.7/11.1/12.5 micrometer channels used for infrared bands 9 - 12.

Table C2

## MAMS flight information for 1987.

| Date     | Times<br>(GMT) | Location | Comments                       |
|----------|----------------|----------|--------------------------------|
| 4-30 (3) |                | CA       | U2, Test flight before Deploy  |
| 5-29 (3) |                | Wallops  | U2, Test flight over coastline |
| 6- 2 (2) | 0130-0400      | *MD/VA   | U2, Flight over Raman lidar    |
| 6- 4 (3) | 1330-1945      | *KS      | U2, day, 3 passes              |
| 6- 5 (3) | 0130-0800      | *KS      | U2, night, 5 passes            |
| 6- 6 (2) | 0130-0400      | *MD/VA   | U2, Flight over Raman lidar    |
| 6- 7 (2) | 0130-0400      | *MD/VA   | U2, Flight over Raman lidar    |

Table C3

## MAMS flight information for 1988.

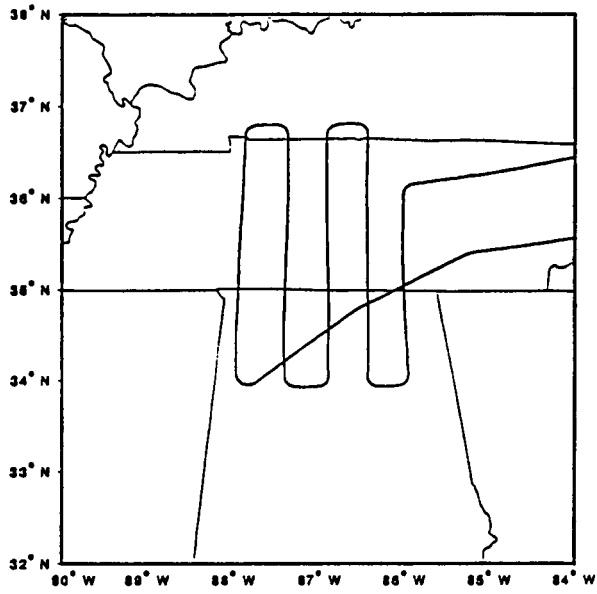
| Date     | Times<br>(GMT) | Location | Comments                       |
|----------|----------------|----------|--------------------------------|
| 1-10 (3) |                | CA       | ER2, Test flight, Tbb drop     |
| 1-27 (3) | 1441-1657      | LA       | ER2, Geomorph., Tbb drop       |
| 6- 5 (2) | 1504-1703      | *VA      | ER2, Test flight, Tbb drop     |
| 6-10 (2) | 1500-2030      | *AL      | ER2, Moist. mapping, Tbb drop  |
| 6-27 (2) |                | VA       | ER2, Test flight, good data    |
| 6-28 (2) |                | AL       | ER2, no data                   |
| 6-30 (2) |                | VA       | ER2, piggy back flight         |
| 7- 5 (2) |                | VA       | ER2, engineering flight        |
| 7- 8 (2) | 1330-1912      | *AL      | ER2, Moist. mapping, good data |
| 8-18 (2) | 1331-1810      | *AL      | ER2, River breeze              |
| 8-25 (3) | 1302-1913      | *E. TN   | ER2, Thermal flux              |
| 8-26 (3) | 1302-1837      | *MS/LA   | ER2, Geomorphc mapping         |

- (1). 6.5/11.1/11.1/12.5 micrometer channels used for the infrared bands 9 - 12.
- (2). 6.5/6.5/11.1/12.5 micrometer channels used for infrared bands 9 - 12.
- (3). 3.7/3.7/11.1/12.5 micrometer channels used for infrared bands 9 - 12.

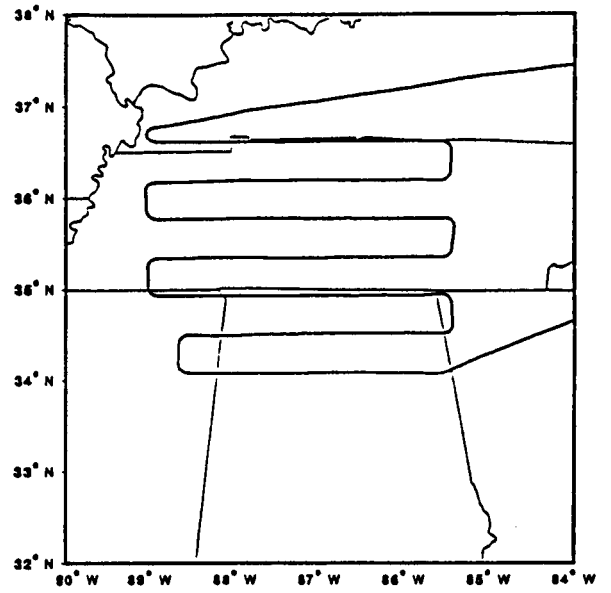
## Appendix D: Selected MAMS Flight Tracks

The Inertial Navigation System (INS) on-board the NASA high altitude aircraft provides accurate positioning information. These data are useful for scene selection and navigating the selected MAMS data scenes. This procedure was discussed in detail in Section IV. The figures below present a number of flight tracks based on the INS data for the flights reported in Appendix C. In the figure captions, the numbers in parentheses are julian dates. Some flight tracks are missing due to recorder malfunction.

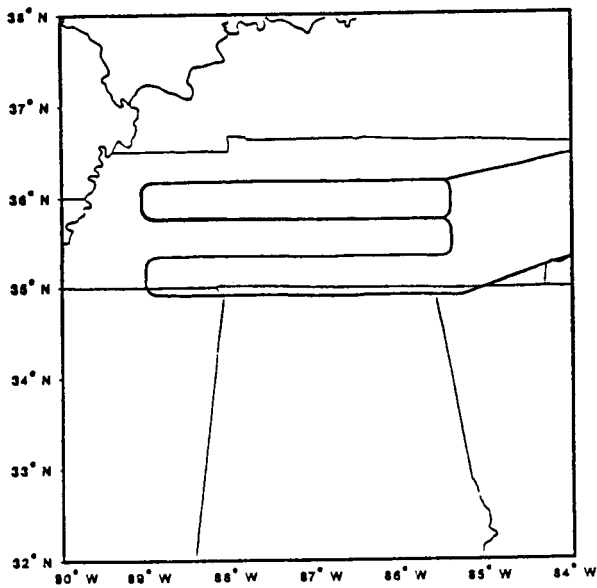
FLIGHT DATE: 86166



FLIGHT DATE: 86169



FLIGHT DATE: 86170



FLIGHT DATE: 86177

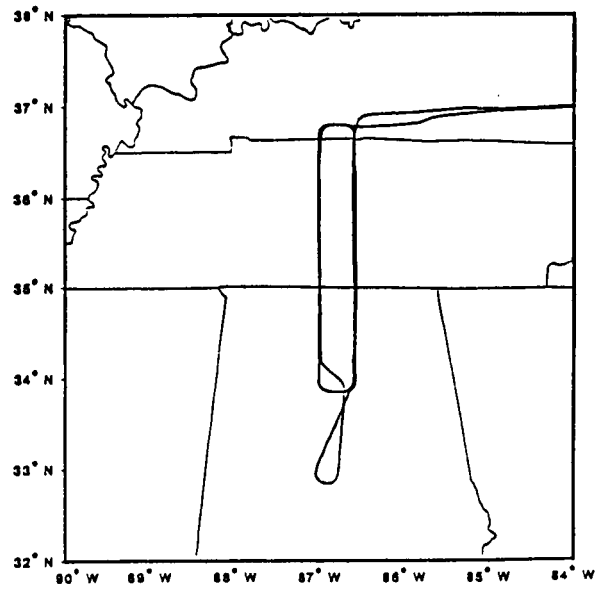


Figure D1. MAMS flight tracks for June 15 (166), 18 (169), 19 (170), and 26 (177) of 1986.

FLIGHT DATE: 86186

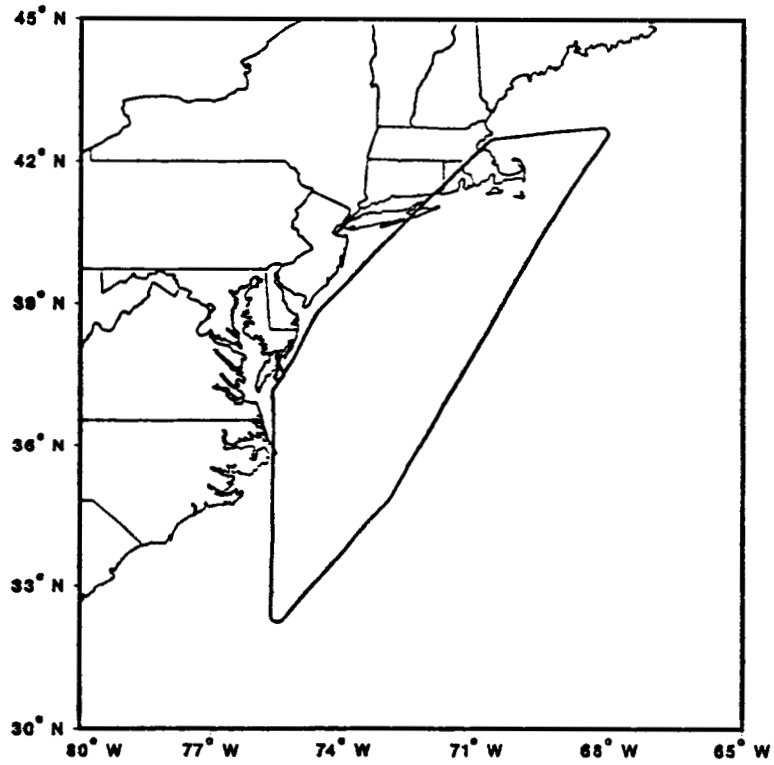
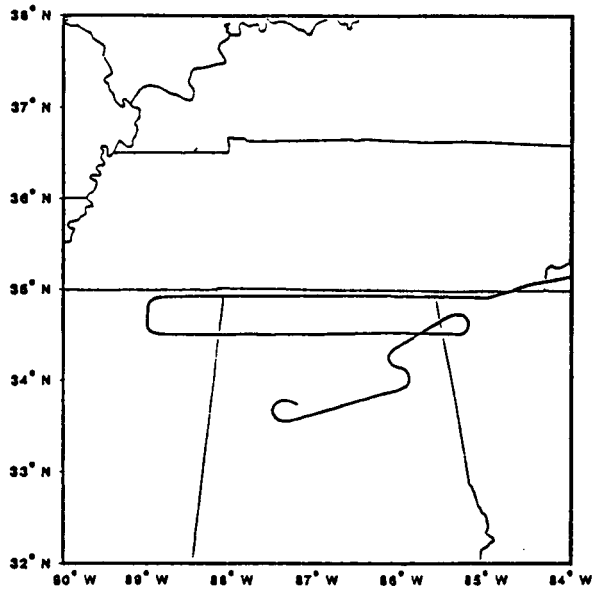
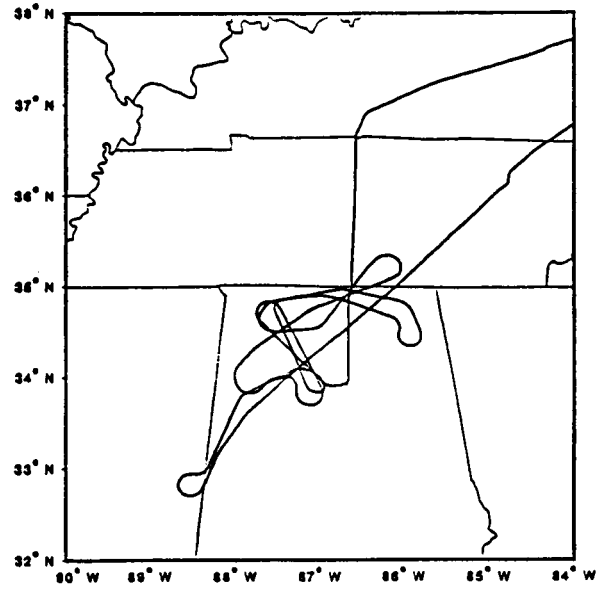


Figure D2. MAMS flight track for July 5 (186), of 1986.

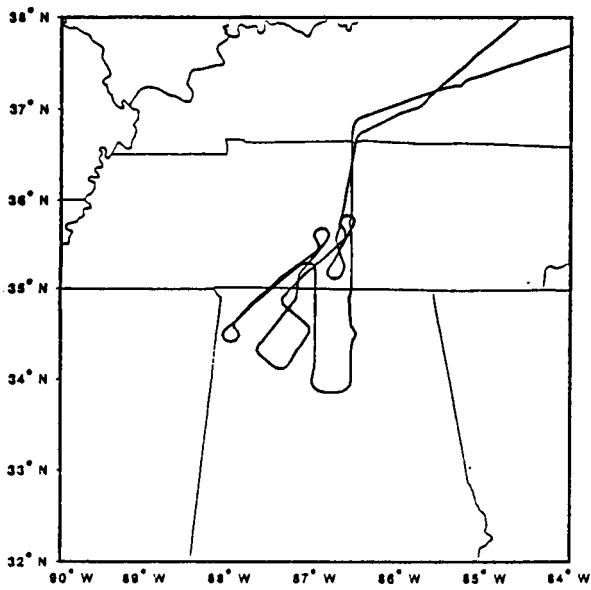
FLIGHT DATE: 86189



FLIGHT DATE: 86192



FLIGHT DATE: 86193



FLIGHT DATE: 86201

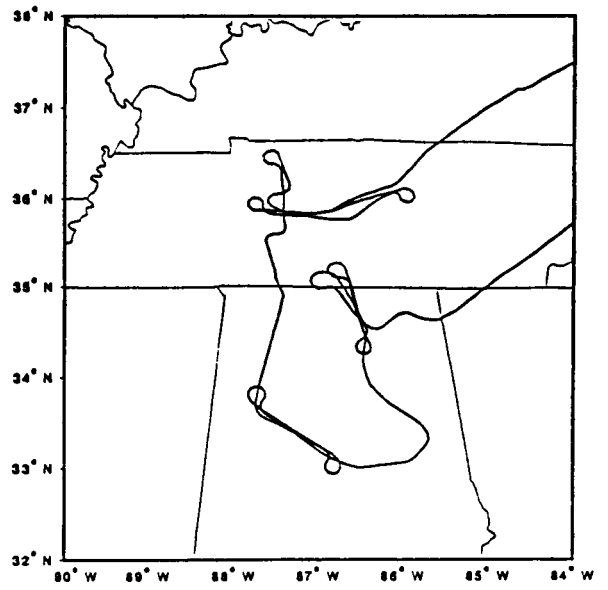


Figure D3. MAMS flight tracks for July 8 (189), 11 (192), 12 (193), and 20 (201) of 1986.

FLIGHT DATE: 86202

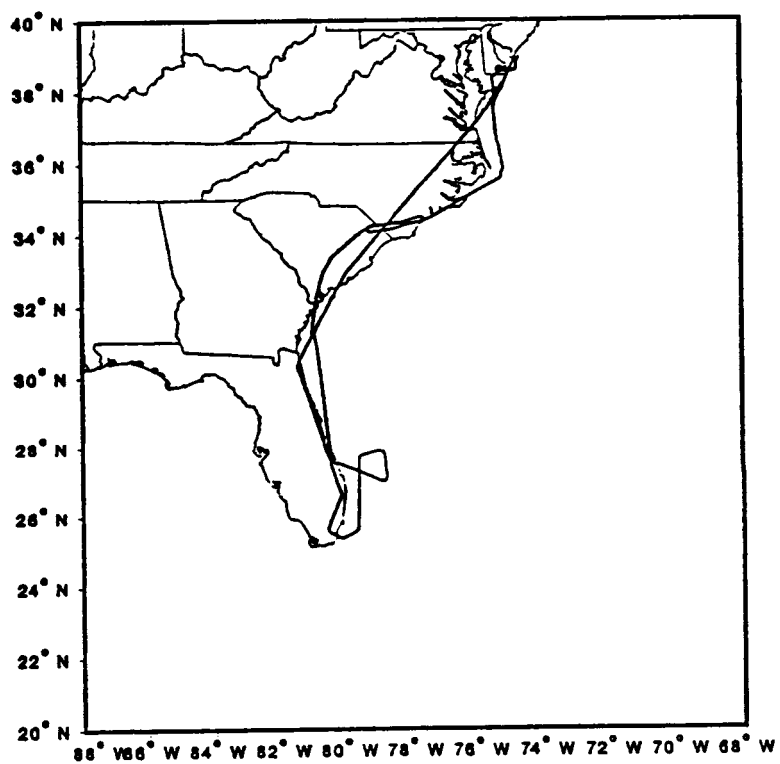
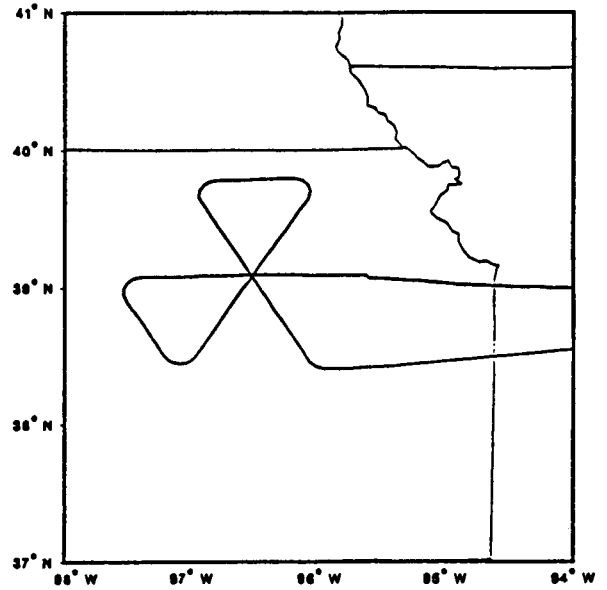
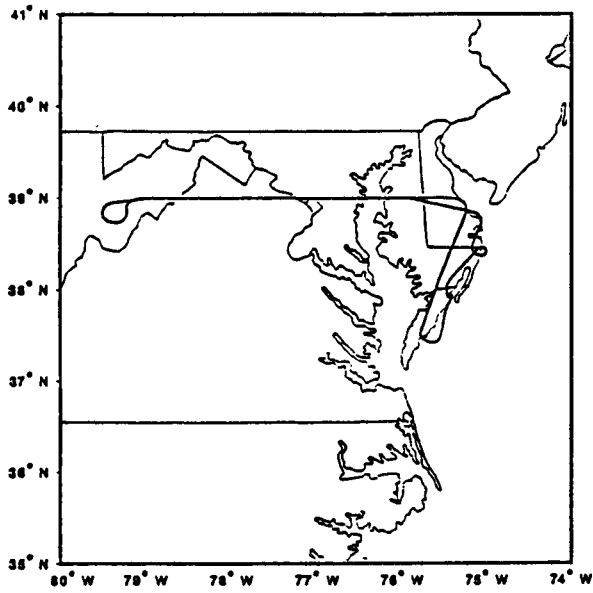


Figure D4. MAMS flight track for July 21 (202), 1986.

FLIGHT DATE: 87153

FLIGHT DATE: 87155



FLIGHT DATE: 87156

FLIGHT DATE: 87157

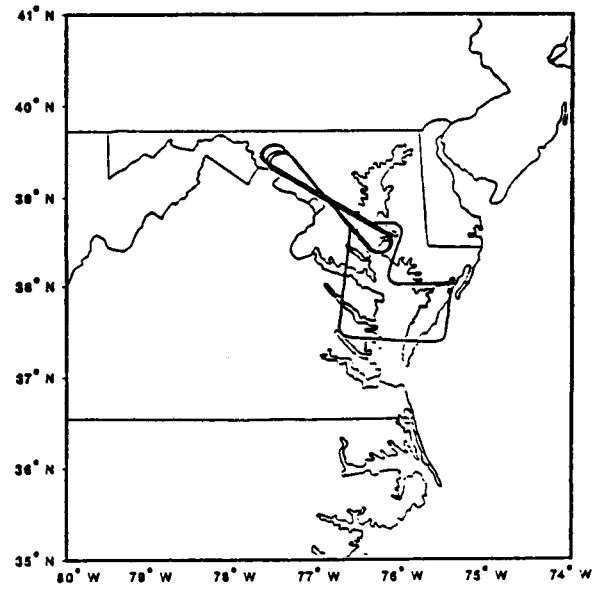
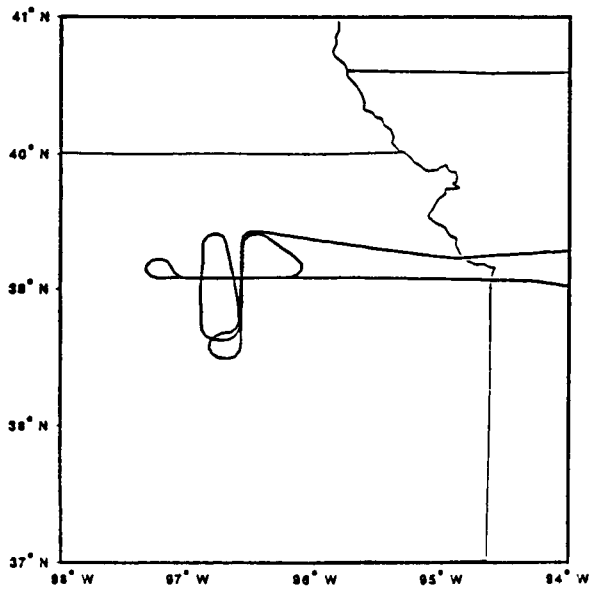
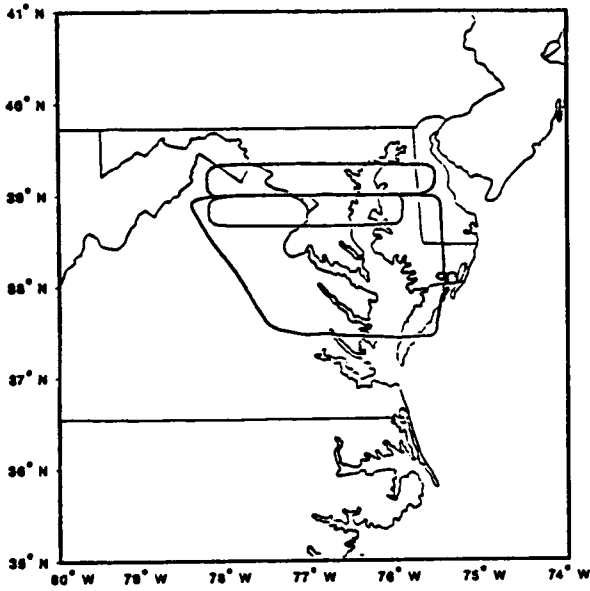
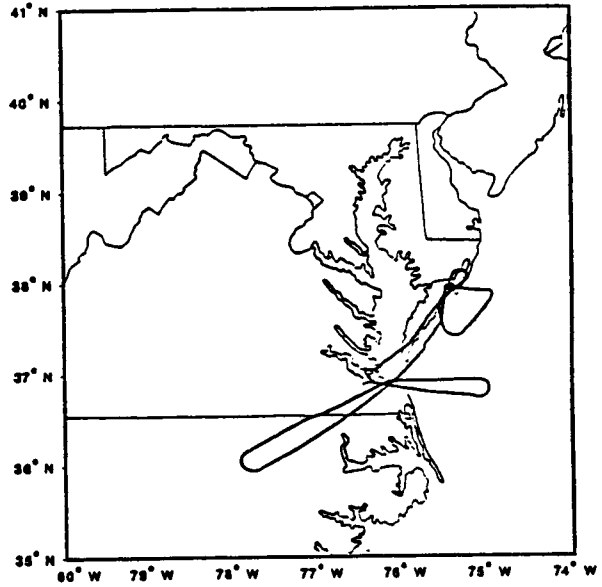


Figure D5. MAMS flight track for June 2 (153), June 4 (155), June 5 (156), and June 6 (157), of 1987.

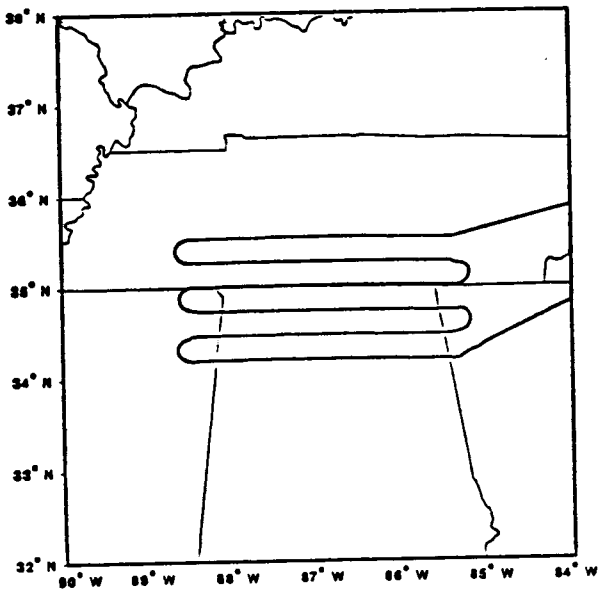
FLIGHT DATE: 87158



FLIGHT DATE: 88157



FLIGHT DATE: 88162



FLIGHT DATE: 88190

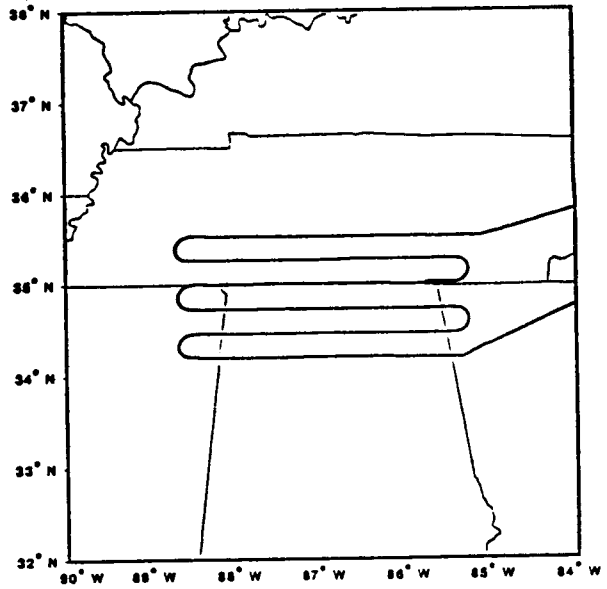
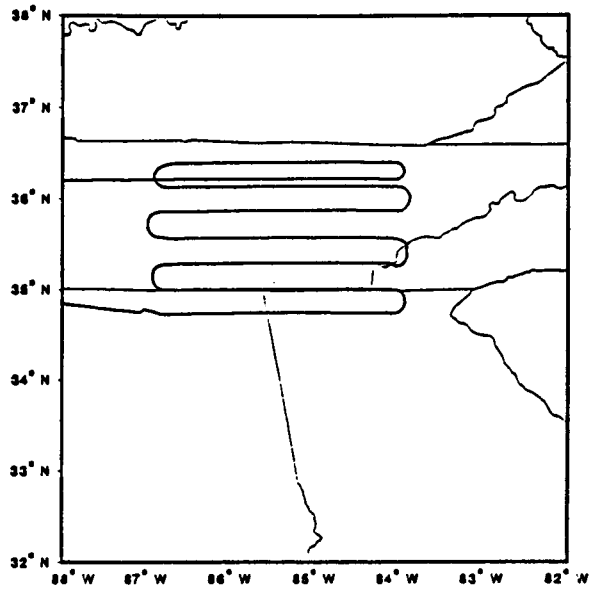
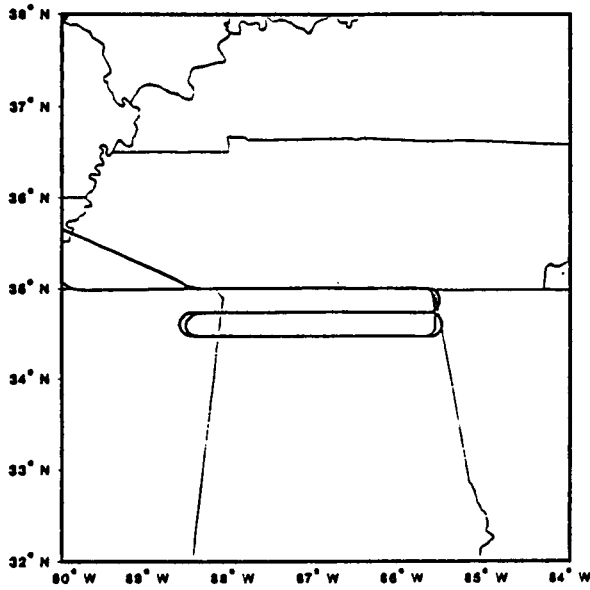


Figure D6. MAMS flight track for June 7 (158), of 1987, June 5 (157), June 10 (162), and July 8 (190), 1988.

ORIGINAL PAGE IS  
OF POOR QUALITY

FLIGHT DATE: 88231

FLIGHT DATE: 88238



FLIGHT DATE: 88239

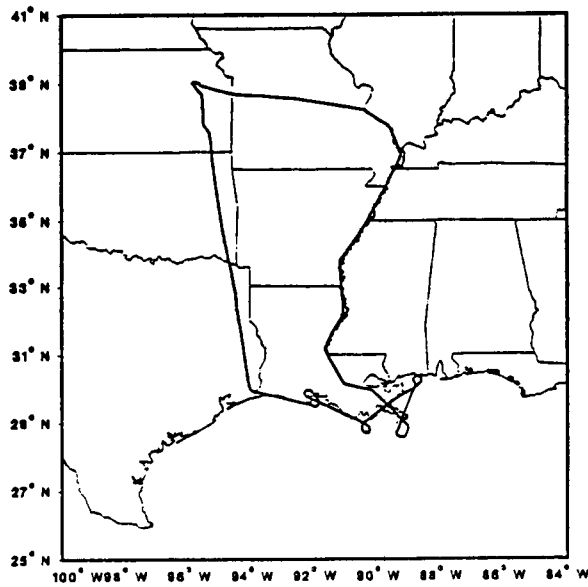


Figure D7. MAMS flight track for August 18 (231), 25 (238), and 26 (239), 1988.

## Appendix E: MAMS Data Requests

A permanent archive of MAMS data is maintained at NASA Ames Research Center. This uncalibrated data can be obtained by contacting

Mr. Jeff Myers  
High Altitude Missions Branch  
NASA Ames Research Center  
Mail Stop 240-12  
Moffett Field, CA 94035  
415-694-6252

Calibrated MAMS data are occasionally provided to external users by Marshall Space Flight Center. Inquiries about the availability of calibrated MAMS data may be addressed to

Dr. Gary J. Jedlovec  
NASA Marshall Space Flight Center  
Remote Sensing Branch, ED 43  
Huntsville, AL 35812  
205-544-5695

Researchers at the University of Wisconsin have archived MAMS data for straight line flight tracks for several of the 1986 COHMEX data sets as part of their ongoing research. These data sets are presented in Table C1 of Appendix C and in Table E1 below. The location of the straight line segments can be seen in

---

Table E1

MAMS Navigated Data Tape Inventory Developed  
by the University of Wisconsin

| Flight Date     | Tape Name | Location        |
|-----------------|-----------|-----------------|
| 6/15/86 (86166) | MC136     | COHMEX Region   |
| 6/18/86 (86169) | MC138     | COHMEX Region   |
| 6/19/86 (86170) | MC140     | COHMEX Region   |
| 6/26/86 (86177) | MC147A    | COHMEX Region   |
| 7/ 3/86 (86184) | MC155     | COHMEX Region   |
| 7/ 5/86 (86186) | MC159     | Atlantic Ocean  |
| 5/29/87 (87149) | M87104    | Delaware Coast  |
| 6/ 4/87 (87155) | M87106    | Kansas (FIFE)   |
| 6/ 5/87 (87156) | M87107    | Kansas (FIFE)   |
| 1/27/88 (88027) | M88034    | Louisiana Coast |

---

the flight track maps of Figs. D1 - D7. The advantage of straight line flight tracks is that accurate location of each pixel can be obtained with navigation software. This data have been made available to MSFC and can be provided to other scientists. Please direct inquiries to Dr. Gary J. Jedlovec at the above address.

## REFERENCES

- Arnold, J. E., (editor), 1986: Satellite Precipitation and Cloud Experiment: Experiment Design Document. Atmospheric Sciences Laboratory, K. E. Johnson Research Center, University of Alabama, Huntsville, 150pgs.
- Hillger, D. W., and T. H. Vonder Haar, 1988: Estimating noise levels of remotely sensed measurements from satellites using spatial structure analysis. J. Atmos. Oceanic Tech., 5, 206-214.
- Hillger, D. W., and T. H. Vonder Haar, 1979: An analysis of satellite infrared soundings at the mesoscale using statistical structure and correlation functions. J. Atmos. Sci., 36, 287-305.
- Jedlovec, G. J., 1988: Determination of low-level precipitable water variability from split window channel radiance data. Preprints Third Conference on Satellite Meteorology and Oceanography, AMS, Boston, 89-94.
- Jedlovec, G. J., 1987: Determination of atmospheric moisture structure from high resolution MAMS radiance data. Ph.D. Thesis, The University of Wisconsin-Madison, available University Microfilms International, P. O. Box 1764, Ann Arbor, MI 48106, 173pg.
- Jedlovec, G. J., W. P. Menzel, R. Atkinson, G. S. Wilson, and J. Arveson, 1986a: The Multispectral Atmospheric Mapping Sensor (MAMS): Instrument Description, Calibration, and Data Quality. NASA Technical Memorandum 86565, Marshall Space Flight Center, Huntsville, AL. 37pgs.
- Montgomery, H. E., and L. W. Uccellini (ed.), 1985: VAS Demonstration: (VISSR Atmospheric Sounder) Description and Final Report. NASA Reference Publication 1151, 198pgs.
- NASA, 1988a: MODIS: Moderate-Resolution Imaging Spectrometer: Instrument Panel Report. Eos Announcement of Opportunity, Volume IIb, 59pgs.
- NASA, 1988b: Airborne Science Newsletter, 88-1, March, avail. Code EM, NASA Headquarters, Washington, DC, 20024, 8pgs.
- Schwalb, A., 1982: The TIROS-N/NOAA A-G Satellite Series. NOAA Technical Memorandum NESS 95, Washington, D.C., 75pgs.
- Sellers, P. J., and F. G. Hall, 1987: First ISLSCP Field Experiment (FIFE): Experiment Plan, Available Goddard Space Flight Center, 177 pgs.
- Smith, W. L., H. M. Woolf, H. B. Howell, H. E. Revercomb, and H.-L. Huang, 1988: High resolution Interferometer Sounder - The retrieval of atmospheric temperature and water vapor profiles. Preprints Third Conference on Satellite Meteorology and Oceanography, AMS, Boston, 266-271.
- Suomi, V. E., R. Fox, S. S. Lemaye, and W. L. Smith, 1983: McIDAS III: A modern interactive data access and analysis

system. J. Climo. Appl. Meteor., 22, 765-778.  
Wilson, G. S., R. J. Curran, and D. M Butler, 1988: NASA's Earth  
Science Geostationary Platform. Third Conference on  
Satellite Meteorology and Oceanography, AMS, Boston,  
272-277.

## BIBLIOGRAPHY

- Arnold, J. E., (editor), 1986: Satellite Precipitation and Cloud Experiment: Experiment Design Document. Atmospheric Sciences Laboratory, K. E. Johnson Research Center, University of Alabama, Huntsville, 150pgs.
- Hillger, D. W., and T. H. Vonder Haar, 1988: Estimating noise levels of remotely sensed measurements from satellites using spatial structure analysis. J. Atmos. Oceanic Tech., 5, 206-214.
- Hillger, D. W., and T. H. Vonder Haar, 1979: An analysis of satellite infrared soundings at the mesoscale using statistical structure and correlation functions. J. Atmos. Sci., 36, 287-305.
- Houghton, J. T., F. W. Taylor, and C. D. Rodgers, 1984: Remote Sounding of Atmospheres, Cambridge University Press, 343 pgs.
- Jedlovec, G. J., 1988: Determination of low-level precipitable water variability from split window channel radiance data. Preprints Third Conference on Satellite Meteorology and Oceanography, AMS, Boston, 89-94.
- Jedlovec, G. J., 1987: Determination of atmospheric moisture structure from high resolution MAMS radiance data. Ph.D. Thesis, The University of Wisconsin-Madison, available University Microfilms International, P. O. Box 1764, Ann Arbor, MI 48106, 173pg.
- Jedlovec, G. J., W. P. Menzel, R. Atkinson, G. S. Wilson, and J. Arveson, 1986a: The Multispectral Atmospheric Mapping Sensor (MAMS): Instrument Description, Calibration, and Data Quality. NASA Technical Memorandum 86565, Marshall Space Flight Center, Huntsville, AL. 37pgs.
- Jedlovec, G. J., W. P. Menzel, G. S. Wilson, and R. J. Atkinson, 1986b: Detection of mountain induced mesoscale wave structures with high resolution moisture imagery. Second Conference on Satellite Meteorology/ Remote Sensing and Applications, AMS, Boston, 365-369.
- Liou, K., 1980: An Introduction to Atmospheric Radiation. Academic Press, New York, 392 pgs.
- Menzel, W. P., G. J. Jedlovec, and G. S. Wilson, 1986: Verification of small scale features in VAS imagery using high resolution MAMS imagery. Second Conference on Satellite Meteorology/ Remote Sensing and Applications, AMS, Boston, 108-111.
- Montgomery, H. E., and L. W. Uccellini (ed.), 1985: VAS Demonstration: (VISSR Atmospheric Sounder) Description and Final Report. NASA Reference Publication 1151, 198pgs.
- NASA, 1988a: MODIS: Moderate-Resolution Imaging Spectrometer: Instrument Panel Report. Eos Announcement of Opportunity, Volume IIb, 59pgs.
- NASA, 1988b: Airborne Science Newsletter, 88-1, March, avail. Code EM, NASA Headquarters, Washington, DC, 20024,

- 8pgs.
- Schwalb, A., 1982: The TIROS-N/NOAA A-G Satellite Series. NOAA Technical Memorandum NESS 95, Washington, D.C., 75pgs.
- Sellers, P. J., and F. G. Hall, 1987: First ISLSCP Field Experiment (FIFE): Experiment Plan, Available Goddard Space Flight Center, 177 pgs.
- Smith, W. L., H. M. Woolf, H. B. Howell, H. E. Revercomb, and H.-L. Huang, 1988: High resolution Interferometer Sounder - The retrieval of atmospheric temperature and water vapor profiles. Preprints Third Conference on Satellite Meteorology and Oceanography, AMS, Boston, 266-271.
- Suomi, V. E., R. Fox, S. S. Lemaye, and W. L. Smith, 1983: McIDAS III: A modern interactive data access and analysis system. J. Climo. Appl. Meteor., 22, 765-778.
- Wilson, G. S., R. J. Curran, and D. M. Butler, 1988: NASA's Earth Science Geostationary Platform. Third Conference on Satellite Meteorology and Oceanography, AMS, Boston, 272-277.

APPROVAL

IMPROVED CAPABILITIES OF THE MULTISPECTRAL ATMOSPHERIC  
MAPPING SENSOR (MAMS)

By Gary J. Jedlovec, K. Bryan Batson, Robert J. Atkinson,  
Chris C. Moeller, W. Paul Menzel, and Mark W. James

The information in this report has been reviewed for technical content. Review of any information concerning Department of Defense or nuclear energy activities or programs has been made by the MSFC Security Classification Officer. This report, in its entirety, has been determined to be unclassified.



---

E. TANDBERG-HANSSSEN  
Director  
Space Science Laboratory